Thermal performance of a coupled solar parabolic trough collector latent heat storage unit for solar water heating in large buildings

Bilal Lamrani, Frédéric Kuznik, Abdeslam Draoui

Thermal performance of a coupled solar parabolic trough collector latent heat storage unit for solar water heating in large buildings

Bilal Lamrani [a*], Frédéric Kuznik [a], Abdeslam Draoui [b]

[a] Université de Lyon, INSA-Lyon, CETHIL UMR5008, F-69621 Villeurbanne, France

[b] Faculté des Sciences et Techniques de Tanger, Equipe de recherche en Transferts Thermiques et Energétique (UAE/U10FST), BP 416 Tanger, Maroc

* Corresponding author (Bilal Lamrani): bilal.lamrani@insa-lyon.fr

Abstract

This paper deals with the feasibility of using a coupled solar parabolic trough collector-latent heat thermal energy storage system for large buildings hot water production. A detailed dynamic thermal model is developed to investigate the thermal performance of the studied system under realistic meteorological conditions. The validation of the developed model is carried out through comparing numerical results with existing numerical and experimental data and a good agreement is obtained. Three kinds of phase change materials are studied and the optimal design of the storage system is determined for weather conditions of a typical summer day in the south of France. Both charging and discharging processes of the latent heat storage system are investigated and obtained results show that using the storage system is suitable to provide hot water all the night. These results indicate also that for a mass flow rate of 1800 l/h, using RT-55 as phase change material in the studied system is preferable compared to RT-42 and RT-65. Finally, it is concluded that using the proposed system with RT-55 as storage medium is suitable for large buildings hot water production and the system is able to produce hot water within the ranges of 85-36 °C and 63-38 °C, during daytime and nighttime operation, respectively.

Keywords: Solar Parabolic trough collector; Phase change material, Hot water; Latent heat; large buildings.

1. Introduction

In Europe, building sector, which includes tertiary and housing building, is considered as one of the main energy intensive sector and accounts for 38 % of energy consumption [1].

Due to the requirement of thermal comfort, 85 % of this energy is mainly used for space heating and hot water production. Currently, the energy use for domestic hot water production represents around 15 to 40 % of the total energy needs in buildings [2] which induces greenhouse gas emissions, atmosphere pollution and global warming.

One way to reduce this energy consumption is the use solar energy for hot water production in both tertiary and housing building sectors. In this application, water is heated through converting solar energy into thermal energy using solar water heaters (SWHs). The latter can be classified into three main types: flat plate collectors (FPCs), evacuated tube collectors (ETCs) and concentrated solar collectors [3]. In the literature, FPCs and ETCs are the most commonly used in building sector and are generally coupled to storage systems [4]. In addition, numerical and experimental studies presented by the scientific community are commonly carried out on individual SWH systems to investigate their thermal performance [5–7].

For large buildings, where the consumption of hot water is high such as in commercial building [8,9], hospitals [10], hotels and lodging buildings [11], the integration of SWH systems is also suitable and can contribute successfully to the reduction of the energy consumption and the negative impact of fossil fuels on the environment. In 1993, Pedersen [12,13] have studied the thermal performance and the economic feasibility of a large SWH system for domestic hot water production under weather conditions of Denmark. The studied SWH system consists of 156 m² of FPCs integrated into a large roof to cover a part of the demand of about 150 apartments. The results from these studies showed that the payback time is about ten years and it is necessary to increase the solar collector area per apartment to reach a high yearly solar fraction. Ndoye et al. [14] have studied numerically the effect of integrating FPCs and ETCs for hot water production on the energy consumption in three different types of large buildings. The studied types of reference buildings are: 3-star hotel, residential and office building. They have shown that integrating these solar collectors is beneficial and the greatest amount of avoided CO_2 emissions is observed in hotel building. Colmenar-Santos et al.[15] have investigated the integration of SWHs for hot water production in high-rise buildings. ETCs are selected as SWH system and the studied high-rise building is a five-star hotel in Sao Paulo city (Brazil). Due to the required large amount of hot water for daily operation of the hotel, a large quantity of collector is used with a total area of 320 m². These SHWs are placed at the main entrance canopy of the hotel due to the low roof area. From this study, it has been shown that using SWHs for high consumption buildings such as hotels is suitable and leads to save up 65 % of the electricity cost. Recently, Fertahi et

al. [16] have studied numerically the thermal performance of both FPCs and ETCs equipped with a centralized storage tank and integrated into a large residential building. Dynamic simulation for these SWHs were carried out under weather conditions of Morocco using a total area of 62.124 m². They have shown that using ETCs as SWH system with centralized heat storage is suitable for hot water production compared to FPCs due the high-obtained solar fraction throughout the year.

It should be noted that few studies were conducted so far on hot water production for large buildings and the common used SWHs are either FPCs or ETCs. However, using these type of solar collectors in this application is not beneficial compared to solar concentrator collectors such as solar parabolic through collector (SPTC) [17]. In fact, SPTC gives higher thermal performance compared to the traditional solar collectors and it is able to produce hot water in the range of 50-95°C. In addition to its thermal advantages, it is considered economically viable and recommended for large buildings with 7-day-a-week hot water use [18,19]. The feasibility of using SPTC for hot water production under weather conditions of Cyprus has been conducted by Kalogirou and Lloyd [17]. The studied SPTC model is 1 m² aperture area and it is investigated for domestic and hotel hot water production. Form this study, it is concluded that for individual hot water production, FPCs are suitable compared to SPTCs. However, for large buildings such hotels, SPTCs should be used instead of FPCs due to theirs thermal and economic benefits. The feasibility of using SPTC to produce hot water at low temperature is already studied by several authors [20–25] and they have shown that this solar concentrator is able to produce hot water temperature in the suitable range for building application.

Due to the intermittent nature of solar energy, the use of thermal energy storage with the SPTC for the production of hot water presents a promising solution and could contribute to the reduction of the energy consumption during the off-sunshine hours. Integrating phase change materials (PCMs) with SWHs for domestic application has receiving increasing interest due to its high-energy storage density compared to traditional sensible heat storage [26,27]. Elbahjaoui and El Qarnia [28] have studied numerically a FPC coupled with latent heat thermal energy storage (LHTES) system for individual domestic hot water production. A transient thermal model is developed to predict the thermal behavior of the coupled FPC-LHTES system under weather conditions of Marrakech city (Morocco) and the optimal design of the storage system is determined. They have shown that using the LHTES system is suitable to provide hot water during nighttime operation. They have found also that the mass flow rate of water and the PCM type have a significant effect of the water temperature during

the discharging process. Teamah et al. [29] have incorporated PCM cylindrical modules into a storage tank for hot water production. FPC is used as SWH and coupled with the PCM storage tank. A dynamic thermal model is developed to simulate the functioning of the system using typical weather conditions of Toronto city (Canada). Authors concluded that using PCMs as heat storage medium leads to reduce the storage tank volume by about 50 %. Another study where a FPC is coupled with a LHTES for individual house hot water production is proposed by Haillot et al. [30]. The performance of the studied FPC-LHTES was conducted under weather conditions of Perpignan city (France) and the effect of the PCM on the energy consumption was presented. They have demonstrated that using PCM in the hot water production system leads to increase significantly the system efficiency. Tri Luu et al. [31] studied numerically a coupled ETC-LHTES for domestic hot water production in Queensland (Australia). The performance of the system using PCM is compared with the traditional coupled ETC-water tank. Based on the obtained numerical results, they have shown that using PCM improves the thermal performance of the system and reduces significantly the energy consumption compared to the traditional one.

Recently, Abdelsalam et al. [32] have investigated numerically a FPC coupled with storage tank incorporated with PCMs for hot water production in typical single-family house. The effect of using PCM and its volume on the thermal performance of the system is studied. They confirmed that the integration of PCM in the storage tank leads to increase the solar fraction and to reduce significantly the storage tank volume. Based on the above literature review, most of the proposed studies on SWHs with PCM are focused on hot water production for individual house and using only traditional solar collectors such as FPCs and ETCs. To the best of authors' knowledge, very few studies in the literature have considered solar hot water production for large buildings and most of the proposed studies used only FPCs and ETCs with conventional water storage tank.

Thus, the main contribution of the present work is firstly, to investigate the feasibility of using a SPTC as SWH coupled with a heat storage system in PCMs for large buildings hot water production. Secondly, to develop a transient thermal model to simulate the thermal behavior of the coupled SPTC-LHTES and to determine the optimal design parameters. Finally, to evaluate the thermal performance of the SPTC-LHTES under realistic conditions and to demonstrate the effect of some design and operating parameters such as PCM type and water mass flow rate on the produced water temperature.

The structure of the present paper can be summarized as the following: A detailed description of the proposed SPCT-LHTES system for the production of hot water for large

buildings with its operating strategy are presented in section 2. A thermal dynamic numerical model is developed for both solar concentrator and the heat storage system and is validated in sections 3 and 4. In section 5, an optimization study of the storage system is carried out and the thermal performance of the SPTC-LHTES system using weather conditions of a typical summer day in the south of France are presented and analyzed. Finally, the main findings of the present study are summarized in the conclusion section with some perspectives.

2. System description

The studied hot water production system consists mainly of a SPTC coupled with a well-insulated LHTES system and a circulation pump (**Fig.1**). During the daytime operation (**Fig.1 a**), the SPTC is used to concentrate the heat flux on an absorber in which passes a Heat Transfer Fluid (HTF). A part of the heated HTF (water) is then collected into the storage unit in a closed loop and the rest of HTF is directed to the hot water storage tank. It is worth noting that the present study is focused on the modelling of the coupled solar concentrator PCM storage system and therefore the heat transfer in the hot water storage tank is not considered. During the charging process of the PCM storage system, the heat is transferred by convection and conduction from the heated water to the PCM, which leads to increase its temperature and to store both sensible and latent heat. During the nighttime operation (**Fig.1 b**), the circulation pump between the SPTC and the LHTES is turned off and the circulation of the water coming from the SPTC is stopped. Next, the cold water passes through the thermal energy storage system and the stored heat in the PCM is released and used to produce hot water (discharging process). Through this operation strategy, domestic hot water is produced during both, daytime thanks to the SPTC and nighttime thanks to the LHTES system.

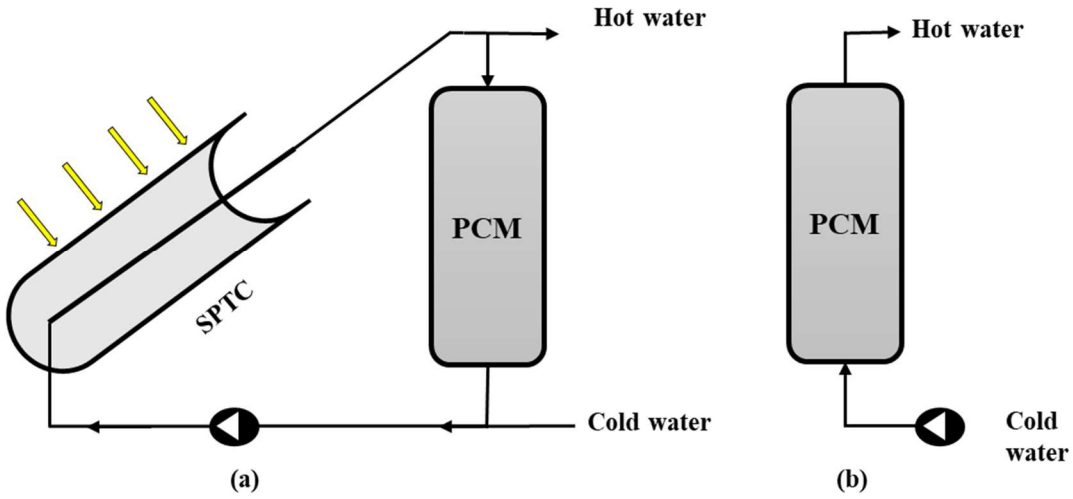

Fig.1 Schematic of the coupled SPTC heat storage system: (a) daytime operation mode, (b) nighttime operation mode.

2.1. Latent heat thermal energy storage system

The proposed storage system consists of a series of cylindrical tubes where the working fluid (water) flows through the inner tubes and the PCM is filled in the shell space (**Fig.2**). Each tube is characterized by an inner radius r_i and a length H (**Fig.2 b**). To reduce heat losses, the sides the LHTES system are well insulated. In the present study, three types of PCM with different melting temperatures are investigated and the optimal number of tubes in the storage system is determined. The characteristics of the studied PCMs are given in **Table1**.

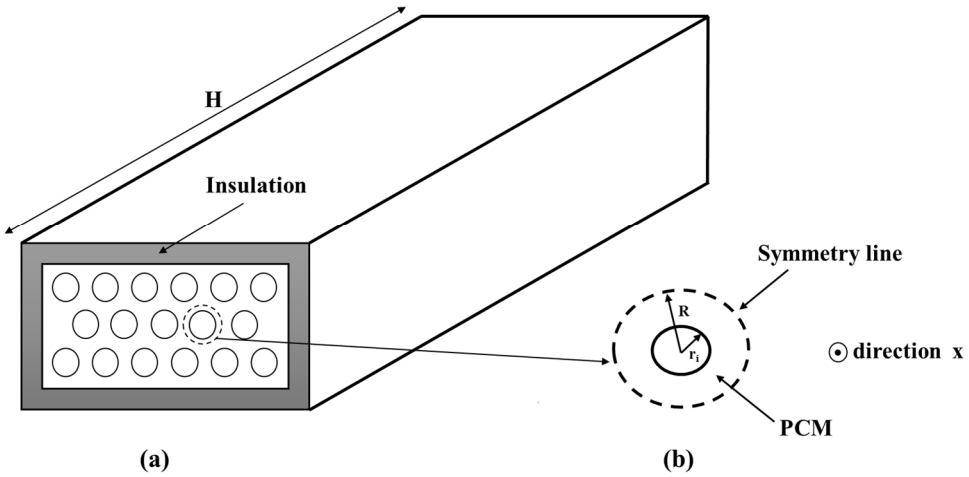

Fig.2 Schematic of the LHTES: (a) Storage system; (b) PCM tube unit.

Table 1 Characteristics of the studied PCM.

	$\rho_s, \rho_l (kg/m^3)$	$C_p (kJ/kgK)$	$k (W/mK)$	$L_s (kJ/kg)$	$T_{melt} (°C)$
RT-42	880-760	2.0	0.2	165	42
RT-55	880-770	2.0	0.2	170	55
RT-65	880-780	2.0	0.2	150	65

2.2. Solar parabolic through collector

As previously mentioned, the SPTC is coupled in a closed loop with the LHTES system to ensure the heat storage process (charging process) during the daytime operation. This solar collector is able to concentrate only beam solar radiation on a receiver tube in which passes a working fluid. More details about the operation principle of the SPTC can be found in

reference [33]. In fact, this type of solar collector has been widely used in several thermal applications [34,35] and it is suitable to provide hot water in particular for large buildings with 7-day-a-week hot water users such as, hospitals, jails and barracks [21,36]. In the present study, the required mass flow rate of hot water in large buildings is fixed at 0.5 kg/s (about 1800 kg/h)[18,19] with a maximal temperature of 85 °C. Based on these operation conditions, the optimal area of the SPTC for the present application is equal to 100 m^2. A schematic diagram of the used SPTC is given in **Fig.3** and its main characteristics are summarized in **Table 2**. Water is used as the working fluid and its thermo-physical properties are given as a function of temperature. These thermophysical properties are taken from [33] and are given in Table 3.

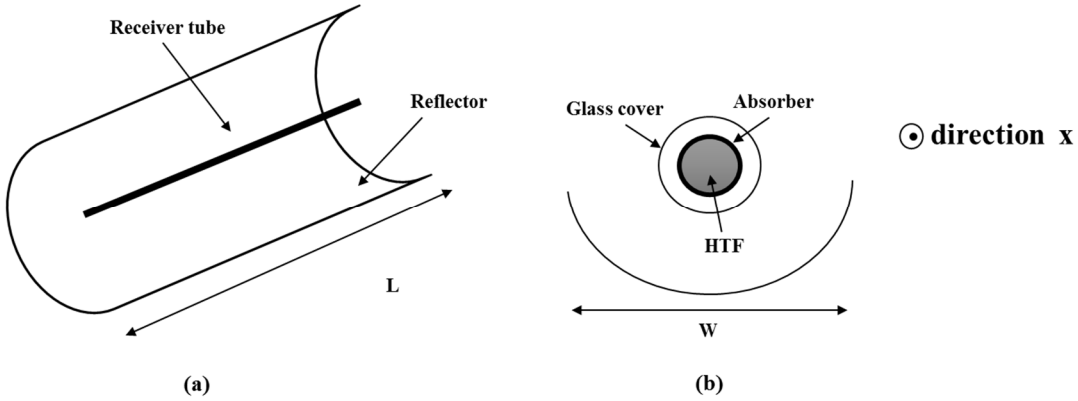

Fig.3 Schematic of concentrator solar collector: (a) components of the SPTC; (b) cross-section of the SPTC.

Table 2. Characteristics the studied SPTC under investigation.

Parameters	Values
Collector Area (W*L)	100 m²
Internal diameter of absorber ($D_{A,i}$)	0.066 m
External diameter absorber ($D_{A,e}$)	0.070 m
Internal diameter glass envelop ($D_{V,i}$)	0.109 m
External diameter glass envelop ($D_{V,e}$)	0.115 m
Thermal absorptance of absorber (α_A)	0.906
Thermal absorptance of glass envelop (α_V)	0.02
Transmittance coefficient of glass envelop (τ_V)	0.95
Emittance coefficient of absorber (ε_A)	0.14
Emittance coefficient of glass envelop (ε_V)	0.86

Table 3. Thermophysical properties of water [33].

$\rho = 1031.84412 + 18.53\ 10^{-3}\ T - 4.68515\ 10^{-4} T^2$

$$k = -0.34149 + 4.97\ 10^{-3}\ T - 6.00979\ 10^{-6}\ T^2$$

$$C_p = 5543.35375 - 8425.29\ 10^{-3}\ T + 0.01305\ T^2$$

$$\mu = 0.03537 - 2.55881\ 10^{-4}\ T + 6.21204\ 10^{-7}\ T^2 - 5.03136\ 10^{-10}\ T^3$$

3. Mathematical modelling

3.1. Modelling of the LHTES unit

The mathematical model of the LHTES system is based on the coupling between transient heat transfer inside the PCM and transient convective heat transfer in the HTF. To model the phase change process inside the PCM, the enthalpy method is used [37,38].

Due to the staggered structure of tubes inside the LHTES system, only a repeating LHTES tube is analyzed (**Fig.2-b**). This LHTES module is delimited by a dotted line (region of symmetry) where the conduction heat flux is null. The same methodology has been used and validated in literature [39–43].

To simplify the developed model, the following assumptions are considered:

- The PCM is considered homogenous and isotropic;
- Natural convection becomes less important in the thin PCM unit as natural convection is constrained, thus its influence during the phase change process is ignored [43,44];
- The thermophysical properties of the PCM are independent of temperature, except the density which is phase-dependent;
- The conductive thermal resistance of the LHTES inner tube is neglected;
- The axial conduction is negligible compared to the thermal convection in the flow.

The energy balance equations are expressed as follows:

- **HTF (water):**

$$\left(\rho C_p\right)_f \pi r_i^2 \frac{\partial T_f}{\partial t} = -\frac{\dot{m}_f}{N_p} C_{p,f} \frac{\partial T_f}{\partial x} + h_c 2\pi r_i \left(T_{m,(r=r_i)} - T_f\right) \quad (1)$$

- **PCM:**

$$\left(\frac{\partial h}{\partial t}\right) = \frac{1}{r}\frac{\partial}{\partial r}\left(ar\frac{\partial h}{\partial r}\right) + \frac{\partial}{\partial x}\left(a\frac{\partial h}{\partial x}\right) - \rho_m L_s \frac{\partial f}{\partial t} \quad (2)$$

Where *h* is the sensible enthalpy and it is given as follows:

$$h(T) = h_{ref} + \int_{T_m}^{T} (\rho C_p)_m dT \quad (3)$$

With h_{ref} is the reference enthalpy and h_c is the convective heat transfer coefficient calculated at each axial location using the Gnielinski correlation [45].

In addition to the above equations, the initial and the boundary conditions are the following:

- At t = t_0:

$$T_m = T_f = T_{amb} \quad (4\text{-a})$$

- $\forall t >$ t0 (Charging process):

$$T_f(x = 0) = T_{f,in} \quad (4\text{-b})$$

$$\frac{\partial T_m(x = 0, r_i \; to \; R)}{\partial x} = 0 \; ; \; \frac{\partial T_m(x = L, r_i \; to \; R)}{\partial x} = 0 \quad (4\text{-c})$$

$$k_m \frac{\partial T_m(x, r = r_i)}{\partial r} = h_c(T_{m(r=r_i)} - T_f) \quad (4\text{-d})$$

$$\frac{\partial T_m(x, r = R)}{\partial r} = 0 \quad (4\text{-e})$$

With $T_{f,in}$ is the water temperature at the inlet of the LHTES and it is equal to the water outlet temperature of the SPTC during the charging process.

- $\forall t > t_0$ (Discharging process):

During the discharging period of the LHTES system, the same boundary conditions described above are used and the water inlet temperature at the LHTES is assumed equal to ambient air temperature:

$$T_f(x = 0) = T_{amb} \quad (4\text{-f})$$

3.2. Modelling of the SPTC

The transient thermal behavior of the considered SPTC is modeled using energy balances at each of its components. In this mathematical model, the conduction heat transfer in the receiver tube is ignored, the HTF is considered incompressible with unidirectional flow and the system is equipped with a full sun tracking system. The energy equation at each component of the SPTC is given as the following:

- **For the water:**

$$m_f\ C_{p,f}\left(\frac{\partial T_f(x,t)}{\partial t} + v\frac{\partial T_f(x,t)}{\partial x}\right) = Q_u \quad (5)$$

- **For the absorber pipe:**

$$m_A\ C_{p,A}\frac{\partial T_A(x,t)}{\partial t} = Q_{ab} - \left(Q_{cv,int} + Q_{r,int}\right) - Q_u \quad (6)$$

- **For the glass cover:**

$$m_V\ C_{p,V}\frac{\partial T_V(x,t)}{\partial t} = \left(Q_{cv,int} + Q_{r,int}\right) - \left(Q_{cv,ext} + Q_{r,ext}\right) \quad (7)$$

Where:

$$Q_u = h_{cv,f}A_f\left(T_A - T_f\right) \quad (8)$$

$$Q_{cv,ext} = h_{cv,ext}A_V(T_V - T_{amb}) \quad (9)$$

$$Q_{r,ext} = h_{r,ext}A_V\left(T_V - T_{sky}\right) \quad (10)$$

$$Q_{cv,int} = h_{cv,int}A_A(T_A - T_V) \quad (11)$$

$$Q_{r,int} = h_{r,int}A_A(T_A - T_V) \quad (12)$$

$$Q_{ab} = I_d.A_o.\tau_V.\rho_m.\alpha_A.\gamma.k(\theta) \quad (13)$$

With h_{cv} and h_r are the convective heat transfer coefficient and the radiative heat transfer coefficient, respectively. These heat transfers coefficients are taken from [33] and are given in the Appendix.

In addition to the energy governing equations, the initial and the boundary conditions are expressed as follows:

- At $t = t_0$:

$$T_i = T_{amb} \quad (14)$$

Where *i* is the component of the SPTC.

- $\forall t > t_0$:

x = 0:

$$T_f = T_{f,in} \quad (15)$$

x = L:

$$\frac{\partial T_f}{\partial x} = 0 \quad (16)$$

4. Numerical procedure and model validation

4.1. Numerical modelling

Governing equations in both LHTES system and SPTC are discretized using an implicit finite difference method. Integrating **Eq. (1)** in the axial direction leads to obtain the following finite difference equation:

$$T_{f,P} = \frac{\left(\frac{T_{f,P}^{0}}{\Delta t} + \frac{a}{\Delta x} T_{f,W} + bT_{m(r=r_i)}\right)}{\frac{1}{\Delta t} + \frac{a}{\Delta x} + b} \tag{17}$$

Where:

$$a = \frac{\dot{m}_f}{N_p \rho_f \pi r_i^2} \tag{18}$$

$$b = \frac{2h_c}{\left(\rho C_p\right)_f r_i} \tag{19}$$

Where $T_{f,P}^{0}$ is the water temperature at the previous time step.

For the PCM, the differential equation is obtained by integrating **Eq. (2)** for each control volume in the plane (r, x). The obtained system of algebraic equations is given as follows:

$$A_P T_{m,P} = A_E T_{m,E} + A_W T_{m,W} + A_N T_{m,N} + A_S T_{m,S} + Q \tag{20}$$

It is worth noting that during this analysis, the phase change process is considered isothermal and the liquid fraction is updated at each time step using the following expression [37,46] :

$$f_P^{k+1} = f_P^k + \frac{A_P T_{m,P}}{\rho_m L_s r \frac{\Delta r \Delta x}{\Delta t}} \tag{21}$$

The value of the liquid fraction f is corrected if it is greater than 1 or smaller than 0 as follows:

$$\begin{aligned} &f = 1 \text{ if } f \geq 1 \\ &f = 0 \text{ if } f \leq 0 \end{aligned} \tag{22}$$

In order to solve the system of algebraic equations (**Eq. (20)**), the iterative Tri-diagonal Matrix Algorithm is used. It should be noted that **Eq. (20)** and **Eq. (17)** are coupled through **Eq. (4-d)**.

The same numerical methodology is applied for discretizing the governing equations of the SPTC (**Eqs. (5), (6) and (7)**). The obtained system of algebraic equations is written in the following form:

$$[A]\{T\}=\{B\} \tag{23}$$

To determine space-time distribution of the temperature in the SPTC, the system of algebraic equations **(Eq.23)** is solved using the iterative Gauss algorithm.

In order to investigate numerically the performance of the coupled SPTC-LHTES system during both charging and discharging processes, a Fortran program is developed and validated with existing experimental and numerical data in the literature. In this developed numerical code, the iterative calculation is performed for each time step until the convergence criterion is reached as follows [33,37]:

$$Max\left|\frac{\left(T_f\right)_P^k-\left(T_f\right)_P^{k-1}}{\left(T_f\right)_P^{k-1}}\right|<10^{-6} \tag{24}$$

The flow chart of the developed numerical model is given in **Fig.4**.

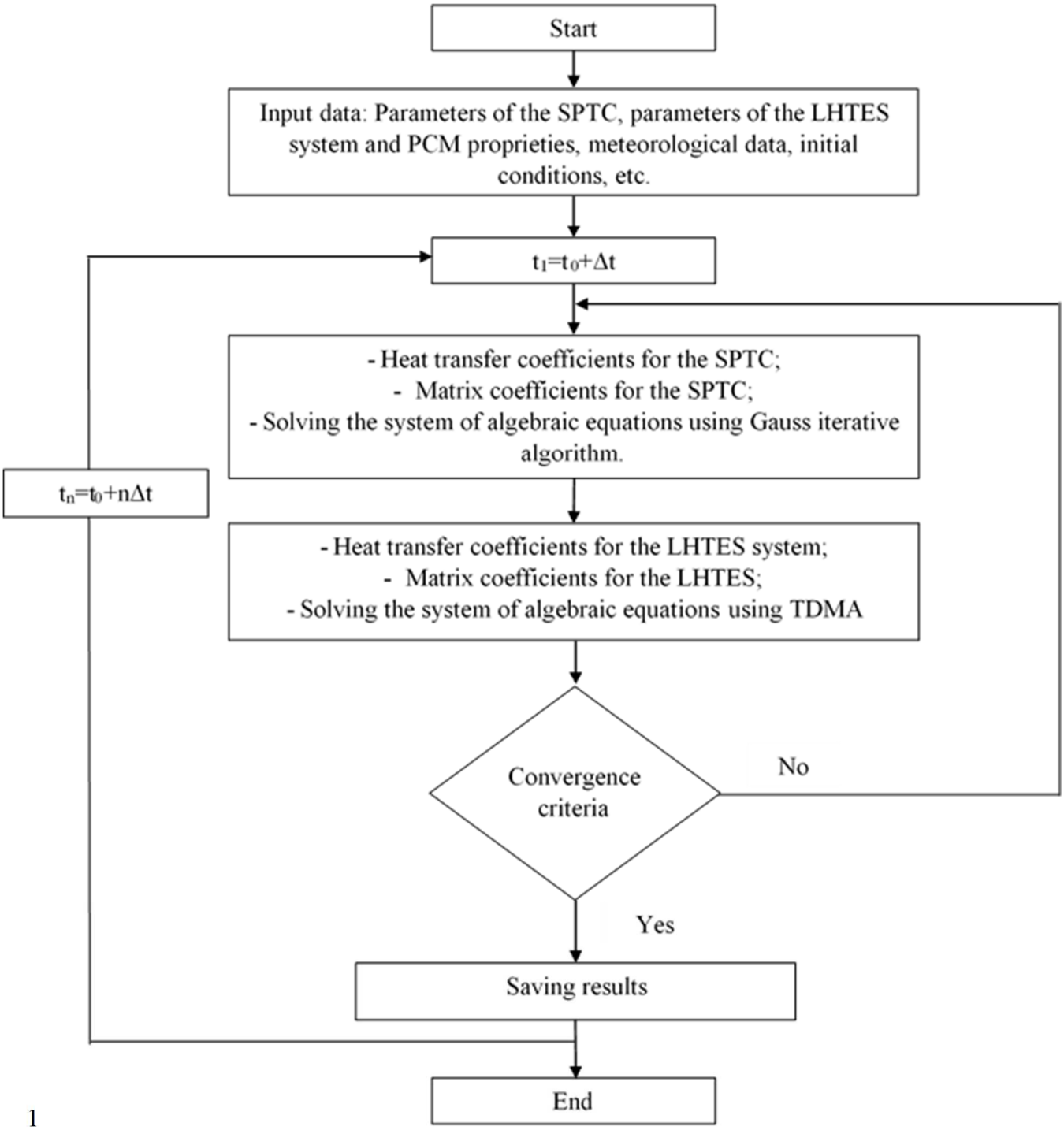

Fig.4 Flow chart of the developed calculation program.

4.2. Grid dependence verification and Model validation

In order to assess the effect of the number of grid on the stability of the numerical scheme and to determine the optimal mesh, five different grids (Nx, Nr) were investigated i.e. (100, 15), (100, 20), (100, 25), (100, 30) and (150, 30). Generally**,** increasing the number of grid leads to increase the result accuracy. However, the calculation time is also increased. From

Fig.5 it can be seen that from the grid (100, 25), there is no significant difference in PCM temperature with a minimal calculation time. In fact, the relative deviation between predicted PCM temperature using the grid (100, 25) and (150, 30) does not exceed 0.18 %. Therefore, this smaller grid, which corresponds to the space steps of $\Delta x = 10^{-2}$ m in the axial direction and $\Delta r = 2.10^{-4}$ m in the radial direction, is adopted in the present numerical study.

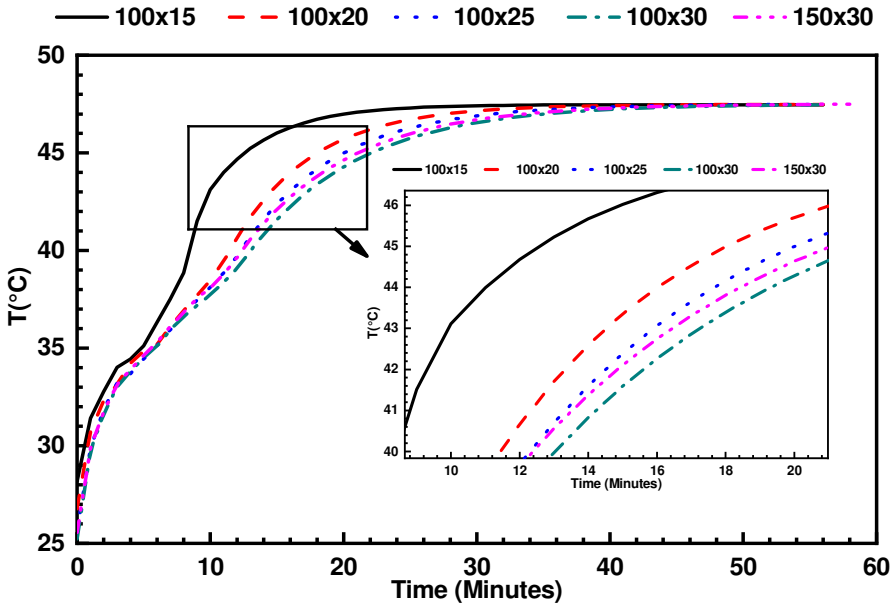

Fig.5 Evolution of PCM temperature: Grid independence verification.

To investigate the validity of the proposed numerical model, a comparative study between the obtained numerical results and experimental results of Lacroix [39] for the LHTES system, experimental data from Sandia National Laboratories (SNL) [47] and numerical results from validated TRNSYS Type 1288 for the SPTC is presented and analyzed.

The experimental study presented by Lacroix [39] is realized on a concentric cylindrical tube similar of that used in the present study and containing n-octadecane as PCM. The length of the inner tube is equal to 1m and is made of copper. The outer tube has an internal diameter equal to 0.0258m and made of plexiglass. In order to reduce the heat losses, the outer cylinder is well insulated. Several thermocouples are installed inside the PCM to measure its temperature during the experimental setup. The same test conditions are used in the present computational model and the obtained results for two different tests (water inlet temperatures: 10 °C and 20 °C above the phase transition temperature of the PCM are presented in **Fig.6**. The analysis of this figure shows that the obtained numerical results are in good agreement with the experimental one and the maximum relative error is about 4.95 %. This small difference between predicted and measured results may be explained by the

negligence of the effect of natural convection during the melting process. Thus, the developed numerical model of the LHTES can be applied to evaluate the performance of the thermal energy storage system under different operation conditions.

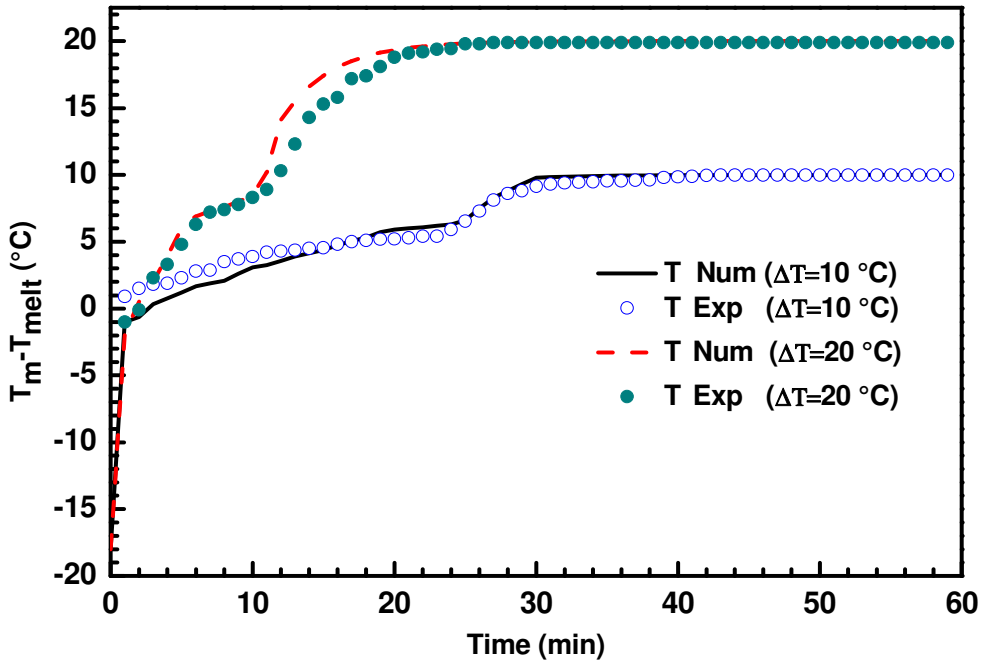

Fig.6 Variation of predicted and measured PCM temperature for two different operation conditions.

To evaluate the validity of the developed numerical model for the SPTC, obtained numerical results are compared with both measured results from the Sandia National Laboratories (SNL) [47] and numerical results from validated TRNSYS model (Type 1288) of the SPTC. The experimental test of SNL is carried out on a solar concentrator similar to that used in the present study. More details about this experimental study can be found in [47]. The comparative study between predicted results and experimental ones shows a good agreement and the maximum discrepancy does not exceed 3% (**Fig.7**).

To assess the viability of the developed SPTC model under transient conditions, a comparative study is carried out between numerical results using the developed model and those from a validated model under TRNSYS 18 software. The latter is based on the dynamic efficiency equation approach and validated using the EN-12975 standard [48]. Weather conditions of a typical summer day in Ajaccio city (41° 55' N, 8° 44' E) are used as input parameters in both models and obtained results are presented in **Fig.8**. It can be seen that the developed numerical model in the present work predicts successfully the real thermal

dynamic behavior of the SPTC under transient conditions. Obtained numerical results are in good agreement with the TRNSYS model one with an average relative error of about 1.5%.

From the detailed validation study presented above, the developed numerical models are suitable to predict the thermal behavior of the SPTC and the LHTES system under different operation conditions.

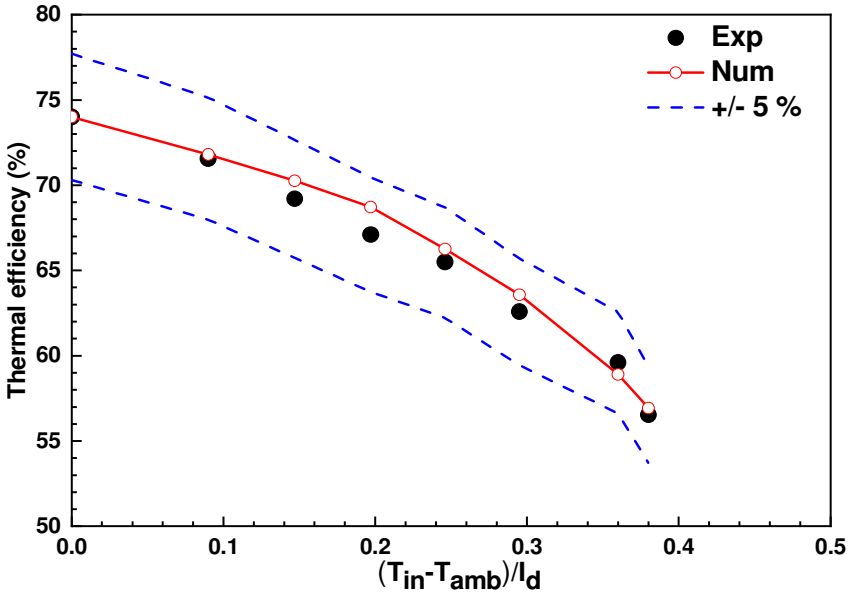

Fig.7 Comparison between numerical results and experimental results of SNL [47].

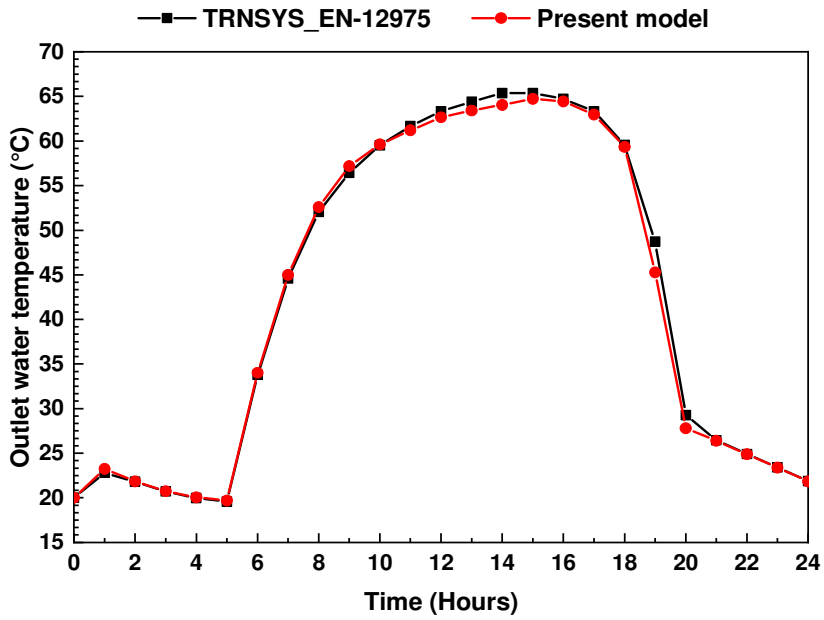

Fig.8. Comparison between numerical results and TRNSYS (Type 1288) results [48] : $A_c = 100$ m², $\dot{m}_f = 0.5$ kg/s.

5. Numerical results and analysis

In this section, the coupled SPTC-LHTES for large buildings hot water production is numerically investigated under climatic conditions of the south of France. Firstly, the optimal amount of PCM and the optimal number tubes in the LHTES is determined for each studied PCM using weather data of a typical sunny day in Ajaccio city. Secondly, the transient thermal behavior of the coupled SPTC-LHTES during both charging and discharging process is investigated. Finally, the effect of the PCM type on the LHTES performance and the feasibility of the hot water production system for large buildings in the south of France are presented and analyzed.

5.1. Optimization study

In order to determine the optimal amount of PCM and the optimal number of tubes in the heat storage system, the PCM liquid fraction at the end of the charging process $(\bar{f})$ and the efficiency of the LHTES (η) are used as performance indicators. The storage system efficiency η can be defined as the following:

$$\eta = \frac{Q_{st}}{\int_0^{t_c} I(\rho\tau_v\alpha_A)A_c dt} \tag{25}$$

Where Q_{st} is the heat stored into the latent form during the charging period t_c and expressed as follow:

$$Q_{st} = \bar{f} M_{PCM} L_s \tag{26}$$

It should be noted that the objective of this optimization study is to determine the optimal number of tubes, which maximizes the efficiency of thermal energy storage. In fact, for each studied PCM, the required PCM volume to run the hot water production system during the off-sunshine hours is calculated first, then the optimal number of tubes to be used is determined. This is obtained when the maximal value of both $\bar{f}$ and η are reached. Generally, if the value of $\bar{f}$ at the end of the charging process is close to one, then the LHTES is fully charged and the thermal efficiency is maximal.

To calculate the PCM volume needed in the hot production system, firstly, the hourly thermal energy needed for the operation of the system is calculated using **Eq.27**. Secondly, the accumulate energy is determined using **Eq.28** and finally the required PCM volume is deduced from **Eq.29** [37,43].

$$Q_f = \dot{m}_f C_{p,f}\left(T_{f,o} - T_{f,in}\right) \tag{27}$$

$$\dot{Q}_{f,total} = \int_0^t Q_f dt \tag{28}$$

$$V_{PCM} = \frac{\dot{Q}_{f,total}}{\rho_s C_{p,s}\left(T_{melt} - T_{f,cold}\right) + \rho L_s + \rho_l C_{p,l}\left(T_{f,hot} - T_{melt}\right)} \tag{29}$$

It is interesting to note that the maximal discharging period is assumed equal to 10 hours. The average inlet cold-water temperature during this period is about 15 °C and the suitable outlet water temperature is assumed equal to 60 °C. **Table 4** presents the accumulated thermal energy over the discharging process and **Table.5** summarizes the required volume for each studied PCM.

Table 4. PCM Storage operation conditions

$\dot{m}_f$(kg/s)	Q_f(kW)	$\dot{Q}_{f,total}$ (GJ),10h	$T_{f,in}$(°C)	$T_{f,o}$(°C)
0.5	94.05	3.3858	15	60

Table 5. Size of the studied PCM storage systems

PCM	V_{PCM} (m^3)	M_{PCM} (kg)	H(m)	r_i (m)
RT-42	13.119	11544.72	5	0.01
RT-55	12.719	11192.72	5	0.01
RT-65	13.478	11860.64	5	0.01

Once the PCM required volume is determined, the optimal number of tubes is calculated using **Eq.30**. It worth nothing that when N_p varies, only the water mass flow rate and the external radius r_e of each PCM tube are affected.

$$N_p = \frac{V_{PCM}}{\pi(r_e^2 - r_i^2)H} \tag{30}$$

As previously mentioned, the present study is carried out using weather conditions of a typical summer day (21 June) in Ajaccio city (41° 55' N, 8° 44' E). This city is characterized by a hot summer Mediterranean climate with an annual sunshine duration ranging from 2500 to 2800 hours. Hourly ambient temperature and DNI received by the solar concentrator during the typical summer day is presented in **Fig.9**. It can be seen that maximal ambient temperature is equal to about 30 °C and the maximal value of DNI is about 860 W/m².

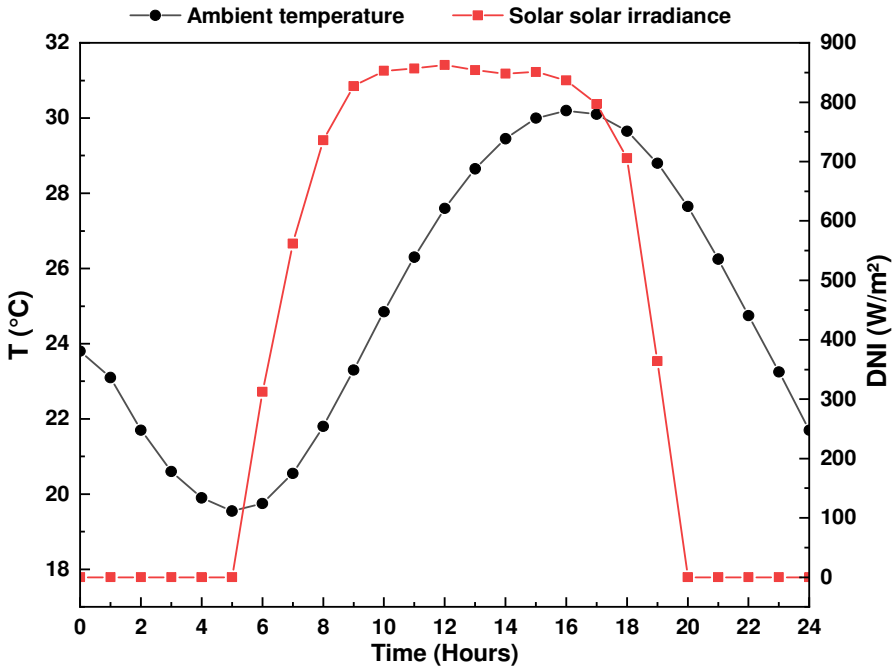

Fig.9 Variation of ambient temperature and DNI received by the SPTC during 21 June in Ajaccio city.

The evolution the LHTES efficiency with the number of tubes is presented if **Fig.10-a** In this case, PCM RT-42 is used as storage medium with a fixed mass equal to 11544.72 kg. Increasing the number of tubes leads to increase the heat transfer exchange between PCM and hot water, however; the mass flow rate in tubes decrease as the number of tubes increases ($\frac{\dot{m}_f}{N_p}$). It can be seen that the storage efficiency increases until reaching a maximal value than it decreases. The optimal number of tubes, which corresponds to the maximal value of LHTES efficiency, is equal to 299 tubes.

The evolution of the PCM liquid fraction during the charging process using the selected optimal number of tubes is presented in **Fig.10-b**. It can be seen that at the beginning of the charging process, the melting of the PCM starts until 6: 00 a.m. and the PCM liquid fraction is close to zero before this hour. During this period, the useful heat by the solar collector is low due to the low solar irradiance received and the temperature of the water thus produced is not high enough to melt the PCM. The PCM during this period stores heat only in the sensible form through the increase of its temperature until the melting temperature. After 6: 00 am and when the useful heat by the solar collector increases, the produced water temperature increases and the melting of PCM begins. During these sunshine hours, the PCM liquid fraction increases and the heat is stored into latent form with time until the end of the charging

process. It should be noted that through using the optimal number of tubes (N_p=299), about 99 % of RT-42 mass is melted at the end of the charging process which corresponds to a maximal LHTES efficiency.

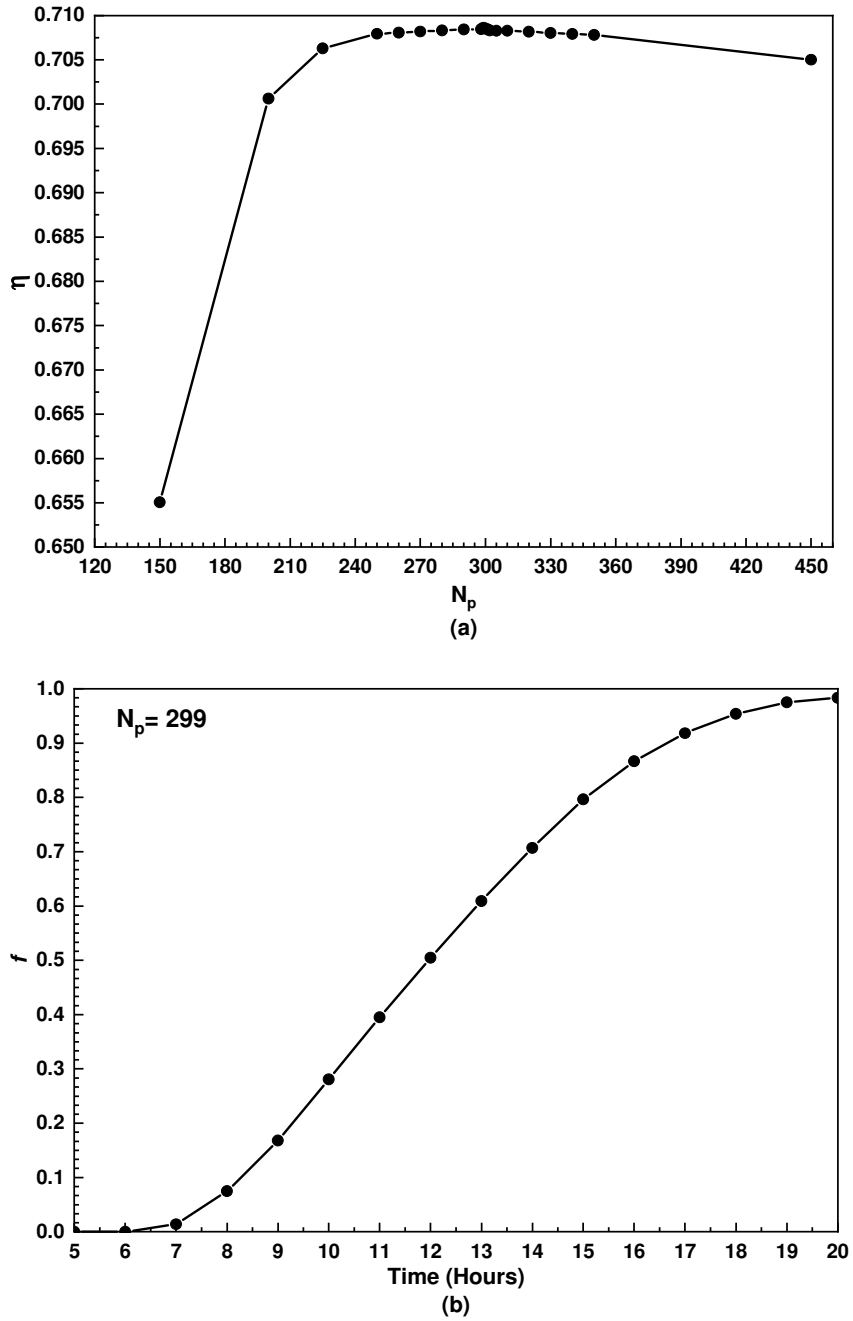

Fig.10. Optimization results for RT 42: (a) Variation of the LHTES efficiency with the number of tubes; (b) Time wise variation of the liquid fraction using the optimal N_p.

The same methodology is adopted for other studies PCMs and the obtained optimal number of tubes are 350 and 310 for RT-55 and RT-65, respectively.

5.2. Transient thermal behavior during charging process

In this section, the thermal behavior of the solar hot water production system using RT-42 as PCM is analyzed during the daytime operation process. It is worth noting that in the following section, the numerical simulations are carried out using the defined optimum parameters in the previous section.

Fig.11 shows the hourly evolution of water temperature at the inlet, middle and outlet of the absorber tube of the SPTC. It can be seen that from 6:00 a.m., the solar collector starts to concentrate solar irradiation on the absorber tube and to produce hot water. A part of the heated water is transferred to the PCM storage tank for charging process and the rest of the hot water is transferred to the hot water storage tank for direct use or storage. It can be seen that the temperature of the water leaving the collector is higher than that in the middle of the SPTC. This behavior is mainly due to the increase in both the rate of heat transfer between the water and the absorber and the residence time of water in the collector with the length of the receiver. Outlet water temperature starts to increase in the morning until reaching a maximum value of 82 °C at 4:00 p.m. The maximum difference between the inlet and the outlet water temperatures is obtained from 10:00 a.m. to 5:00 p.m. and it is about 34 °C, while is equal to zero at 8: 00 p.m. In fact, maximal DNI received by the solar collector is observed from 10:00 a.m. to 5:00 p.m., which correspond to a maximal heat gain by the SPTC. At 8:00 p.m. the DNI received by the solar collector is equal to zero and thus the useful heat gain is also equal to zero.

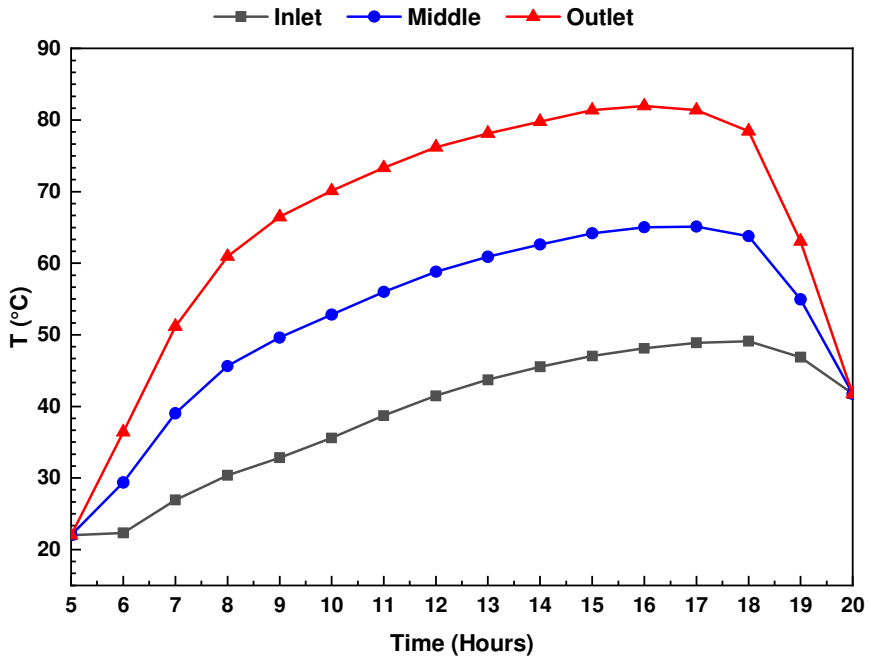

Fig.11. Hourly variation of water temperature in the SPTC during the charging process.

Fig.12 shows the hourly variation of the heat gain by water during the daytime operation of the coupled SPTC-LHTES system. It can be observed that the heat flow recovered by water is minimal during both early morning and late afternoon due to the low values of DNI received by the SPTC. Maximal values of heat gain are obtained when the solar irradiation is maximal and the highest value of heat gain by water is about 72.6 kW reached at noon.

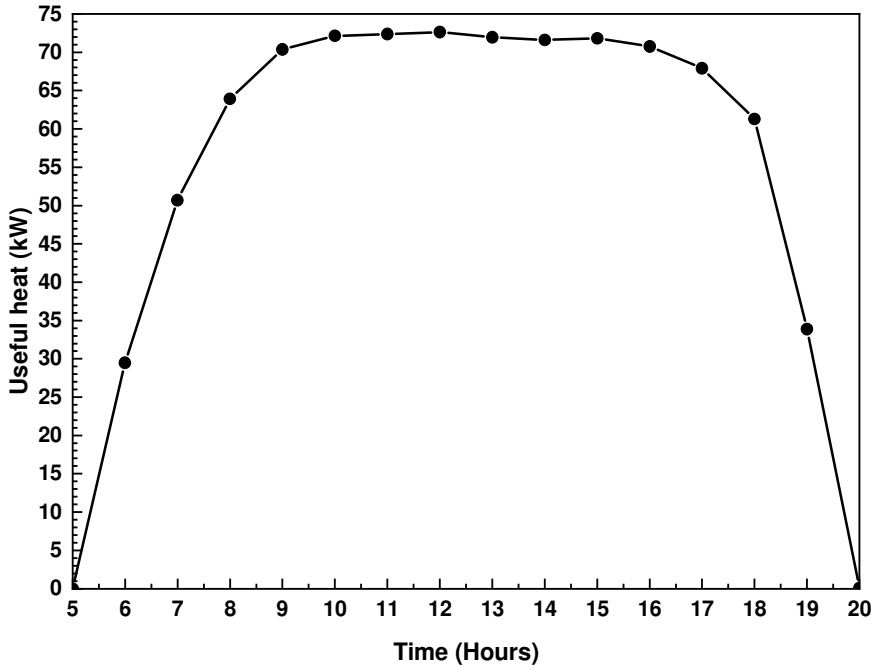

Fig.12 Useful heat gain by water in the SPTC during the charging process.

Fig.13 shows the hourly variation of the PCM temperature and the PCM liquid fraction at three different points in the LHTES unit. These three points are located in H/2 in the axial direction and in r = 0.0112 m, 0.0318 m and 0.0537 m in the radial direction. It can be observed that from 6:00 a.m. to 6:00 p.m., both PCM temperature (**Fig.13-a**) and liquid fraction (**Fig.13-b**) in point r_1 increase faster than those in locations r_2 and r_3. In fact, the PCM in location r_1 is close to the hot water flow compared to r_2 and r_3, which leads to increase its temperature quickly and to change its physical state from solid to liquid during the early morning. However, for r_2 and r_3 and due to the low thermal conductivity of PCM, more time is needed to reach the phase transition temperature (T = 42 °C) and to complete the melting process. After 6:00 p.m., the water temperature at the inlet of the LHTES, which considered equal to the outlet water temperature of the SPTC, starts to decrease (see **Fig.11**) and leads to a rapid reduction of the PCM temperature in r_1 compared to other PCM locations.

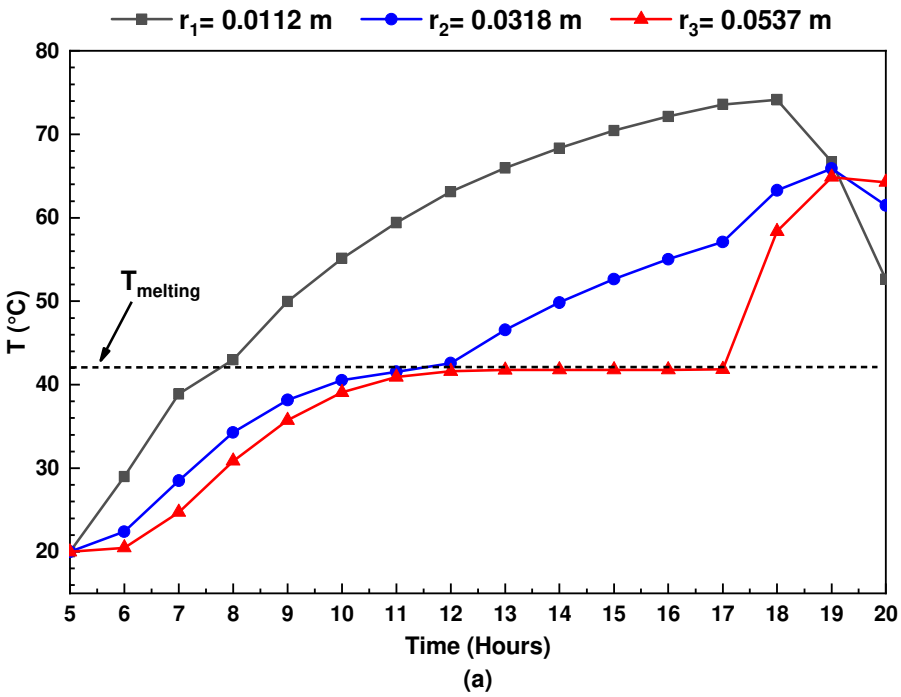

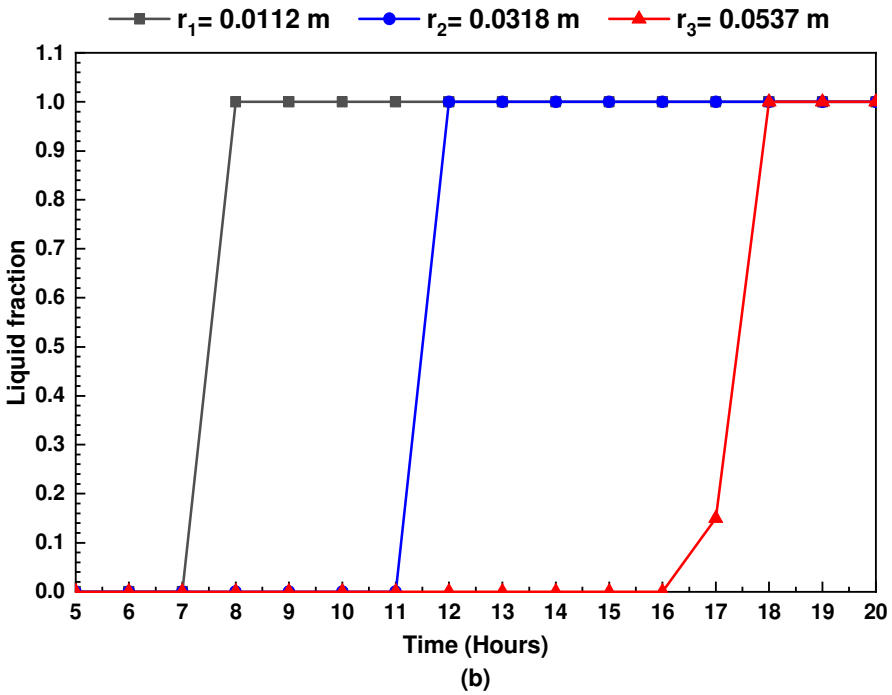

Fig.13 Time wise variation of liquid fraction (a) and PCM temperature (b) at three different locations in the LHTES system.

Fig.14 shows the hourly variation of the total volumetric enthalpy (sensible + latent) in the storage system during the functioning of the coupled SPTC-LHTES. At the begging of the charging process and for a PCM location close to the hot water flow (for example r_1), the amount of stored thermal energy (sensible and latent) increases quickly compared to other

PCM locations far from the hot water flow. It can be seen also that during the phase transition process, the PCM stores a high amount of thermal energy thanks to the latent heat compared the stored sensible heat. Maximal value of total volumetric enthalpy is reached in PCM location r_1 , as it is closer to the hot water flow compared to other locations, and it is about 233 MJ/m^3.

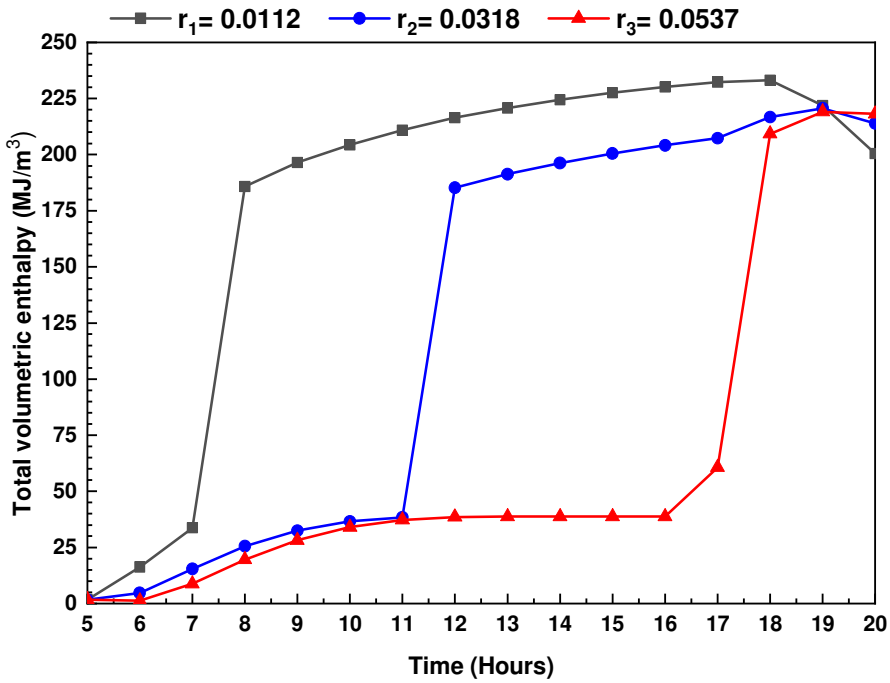

Fig.14 Time wise variation of total volumetric enthalpy in three different locations in the LHTES system.

The time wise variation of the cumulative stored thermal energy in the proposed SPTC-LHTES system during the charging process is presented in **Fig.15**. During the early morning, the thermal energy is stored only into the sensible form due to the increase of the PCM temperature. As time progress and from 07:00 a.m., the melting of PCM begins at some locations, which leads to store thermal energy into both sensible and latent forms. From 10:00 a.m., the amount of stored thermal energy in latent form is higher than that stored in sensible form due to the increase of the amount melted PCM. At the end of the charging process (07:00 p.m.), the cumulative stored thermal energy into latent form is 2.24 times greater than that stored into sensible form and are equal to about 1860 MJ and 830 MJ, respectively. In fact, this result demonstrates the advantage of using PCM as storage medium due to its high-energy storage density compared to the traditional sensible heat storage. Finally, the obtained

stored latent energy is in good agreement with the maximal storage capacity of the used commercial PCM RT-42 ($M_{PCM} \times L_f \approx 1900$ MJ).

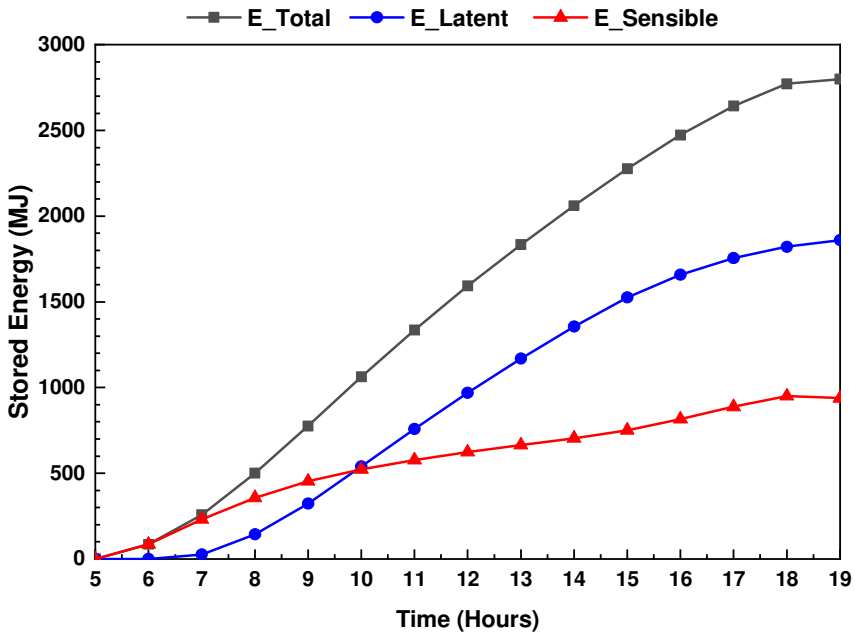

Fig.15 Time wise variation of the cumulative total, latent and sensible stored thermal energy in the LHTES during the charging process of RT-42.

5.3. Transient thermal behavior during discharging process

During the discharging process, assumed to be from 7:00 p.m. to 5: 00 a.m., the circulation of water between the SPTC and the LHTES is stopped. Then, the cold water passes through the LHTES and the stored thermal energy is released to produce hot water. The variation of liquid fraction of PCM RT-42 during the discharging process for seven different mass flow rates is presented in **Fig.16-a**. It can be seen that increasing the mass flow rate of water during the discharging leads to solidify quickly the PCM. This behavior is explained by the increase of the transferred heat rate from PCM to water with the mass flow rate. However, increasing the water mass flow leads also to reduce the residence time of water in the LHTES system. From **fig.16-b**, it is clear that the outlet water temperature decreases quickly with the increase of the mass flow rate due to the reduction of the water residence time. For a low value of mass flow rate (0.15 kg/s for example), about 35 % of PCM RT-42 in the LHTES system is not solidified at the end of the discharging process and the outlet water temperature is approximately equal to the melting temperature all the night. For an optimal functioning of the proposed PTC-LHTES during the discharging process, the liquid fraction at the end of the discharging process must be minimal while the water outlet temperature must be maximal all

the night. Based on this criterion, the suitable mass flow rate of water during the discharging process of RT-42 is 0.25 kg/s with a liquid fraction at the end of the discharging process of about 0.17. The correspond water outlet temperature varies between 65 °C and 28 °C all the night.

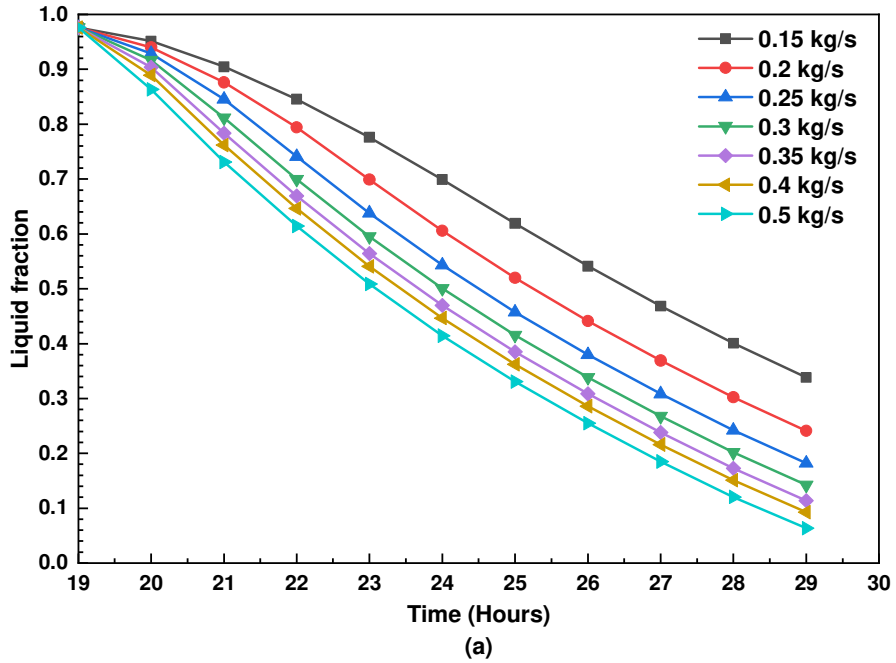

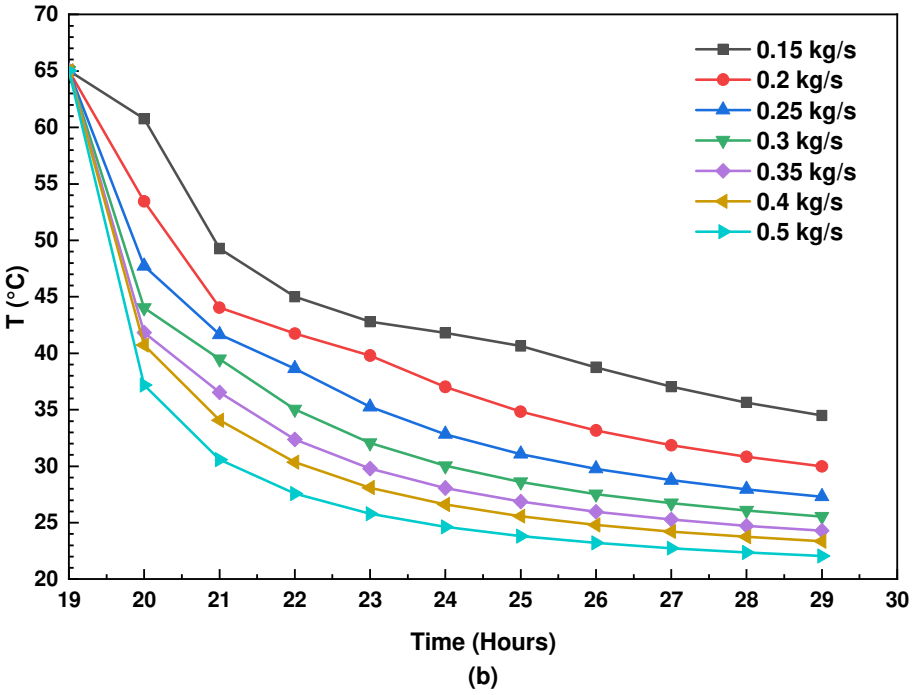

Fig.16 Time wise variation of average PCM liquid fraction (a) and water temperature at the outlet of the LHTES system (b) during the discharging process of RT-42.

Using the selected optimal mass flow rate for RT-42 ($\dot{m}_f$= 0.25 kg/s), the evolution of total volumetric enthalpy at r_2 = 0.0318 m during the discharging process is given in **Fig.17**. At the beginning of the discharging process, only sensible heat is released and transferred to the cold water as the PCM temperature still high than the phase change temperature. When the PCM temperature reaches the phase transition point (about 42 °C), the stored latent heat is released and leads to produce hot water. After the complete solidification process (PCM temperature lower than 42 °C), the PCM temperature continues to decrease and the heat is transferred to the water only into the sensible form.

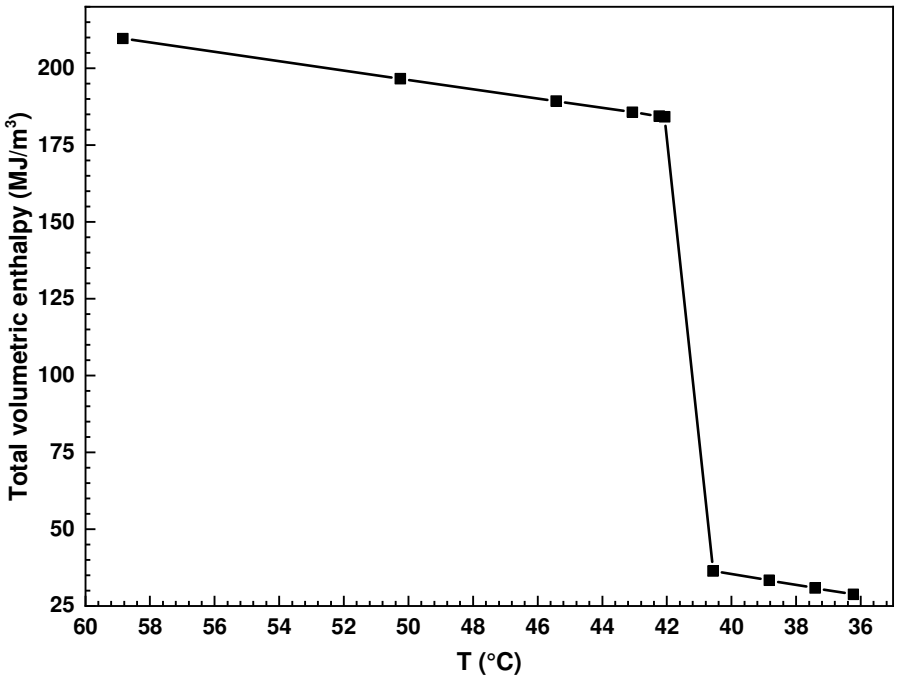

Fig.17 Evolution of total volumetric enthalpy with PCM temperature during the discharging process: $\dot{m}_f$= 0.25 kg/s

5.4. PCM effect on SPTC-LHTES performance

On order to study the effect of the PCM type on the SPTC-LHTES performance, the three studied PCMs, RT-42, RT-55 and RT-65, are investigated. For each PCM, the optimal design parameters determined previously are used and the performance of the system during both charging and discharging process is compared.

Fig.18 illustrates the time wise variation of the latent heat stored/released and the average liquid fraction for the three studied PCMs during charging and discharging process. It should be noted that in this analysis the water mass flow rate is equal to 0.5 kg/s and 0.25 kg/s during the charging and the discharging process, respectively. It can be seen in **Fig.18-a** that during

the melting process of PCM, maximal amount of latent heat is stored in RT-42 and it is equal to about 1860 MJ. However, for RT-55 and RT-65, the amount of latent heat stored at the end of the charging process is 1592.68 MJ and 1134.45 MJ, respectively. This result is due to the amount of melted PCM at the end of the charging process (**Fig.18-b**) which it is about 98 %, 83.7 % and 63.7 % for RT-42, RT-55 and RT-65, respectively. In fact, as the amount of melted PCM increases the stored thermal energy in PCM is also increased. It should be noted that for all studied PCMs, the energy input during the charging operation is the same, thus the time required for a complete melting process is minimal for a PCM with low phase transition temperature (RT-42 for example) and maximal for a PCM with high transition temperature (RT-65 for example).

During the discharging process, the stored thermal energy is released to the cold water, which explains the decrease in both heat stored and liquid fraction with time. At the end of the discharging process, the PCM RT-65 is completely solidified, however; for RT-55 and RT-42, a small amount of PCM still in the liquid state. This can be explained by the small amount of melted PCM during the charging process for RT-65 and by the difference between each PCM melting temperature and cold-water temperature.

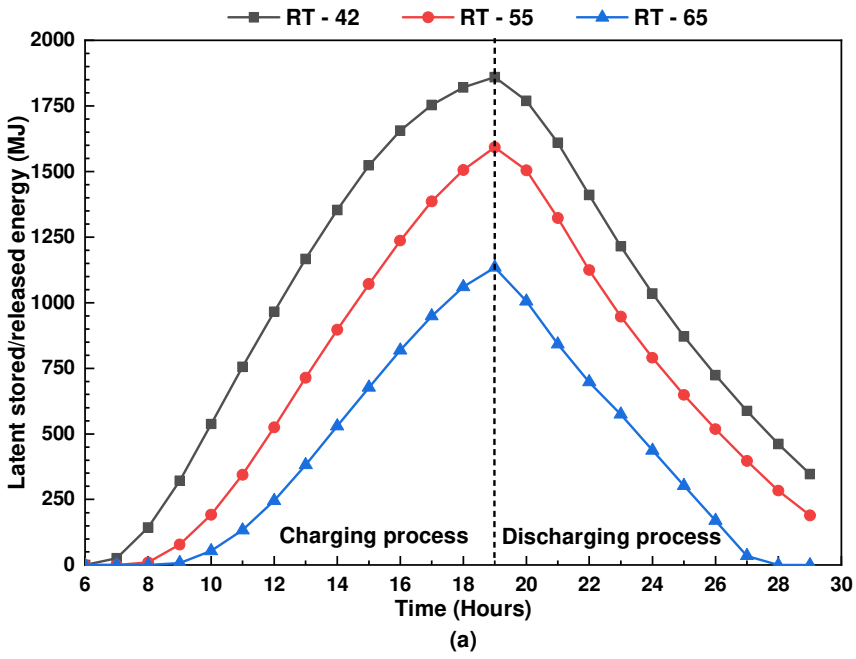

(a)

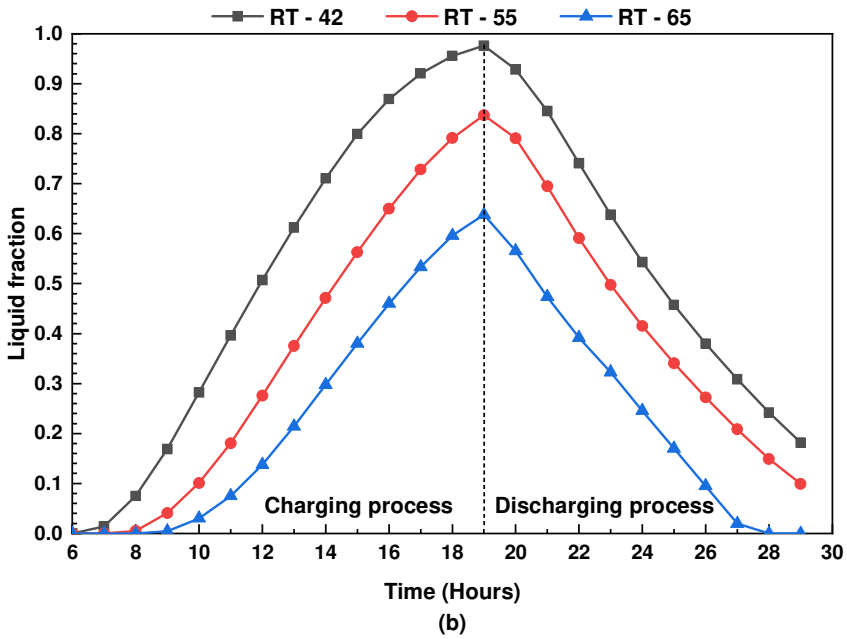

Fig.18 Time wise variation latent heat stored/released (a) and average PCM liquid fraction during the functioning of the SPTC-LHTES.

In practical case of hot water production in large buildings, high amount of hot water with a temperature between 45 °C and 60 °C is required during both daytime and nighttime. For the daytime operation (sunshine hours), the proposed SPTC-LHTES system using the three PCMs is able to produce hot water with a temperature range from 36 °C to 85 °C (**Fig.19**) and with a mass flow rate equal to 0.5 kg/s (about 1800 l/h). This water temperature with a mass flow rate of 1800 l/h is suitable in large buildings and it can be used directly or stored in water tank for later use. For the nighttime operation (off-sunshine hours), the stored sensible and latent heat in PCM is released and it is transferred to the cold water. In fact, the temperature of produced hot water depends on both PCM type and water mass flow rate. To demonstrate the effect of these parameters on water temperature, the hourly variation of water temperature using the three studied PCMs and for three different mass flow rates of water (0.25 kg, 0.375 kg/s and 0.5 kg/s) during the discharging process is given in **Fig.20**. It can be observed that, for the three PCMs, increasing the mass flow rate of water leads to reduce the water temperature during all night. For example, increasing the mass flow rate from 0.25 kg/s (**Fig.20-a**) to 0.5 kg/s (**Fig.20-c**) using RT-42 as PCM, leads to decrease the average water temperature by about 30 % all the night. Indeed, increasing the water velocity increases the convection heat transfer in the storage system, however; this behavior is obviously due the reduction of the water residence time in the LHTES with the increase of the water mass flow rate.

It is true that about of 98 % of PCM RT-42 is melted during the charging process (**Fig.18-b**). However, for hot water production in large buildings where the required mass flow rate is about 0.5 kg/s, this PCM is not beneficial. In fact, for this fixed mass flow rate (0.5 kg/s), the water outlet temperature using RT-42 still lower than the suitable water temperature (between 45 and 60 °C) all the nigh and its varies between 37 °C and 22 °C (**Fig.20-c**). For RT-65, the outlet water during the discharging process varies within the range 68 - 45 °C. However, a high amount of this PCM is not melted during the charging process (about 37 %) which is not practically beneficial for the proposed SPTC-LHTES as this PCM quantity still useless. Based on the suitable water temperature for large buildings and its associated mass flow rate, using RT-55 as PCM in the proposed SPTC-LHTES is suitable compared to both PCMs RT-42 and RT-65. It can be shown clearly in **Fig.20-c** that the produced water temperature during all the night is within the range 38 - 63 ° C through using PCM RT-55 for a mass flow rate of 0.5 kg/s. In order to improve the heat transfer in this RT-55 and to complete both the melting process during the charging process and the solidification process during the discharging process, several heat transfer heat enhancement techniques can be investigated and deserve a detailed separate study.

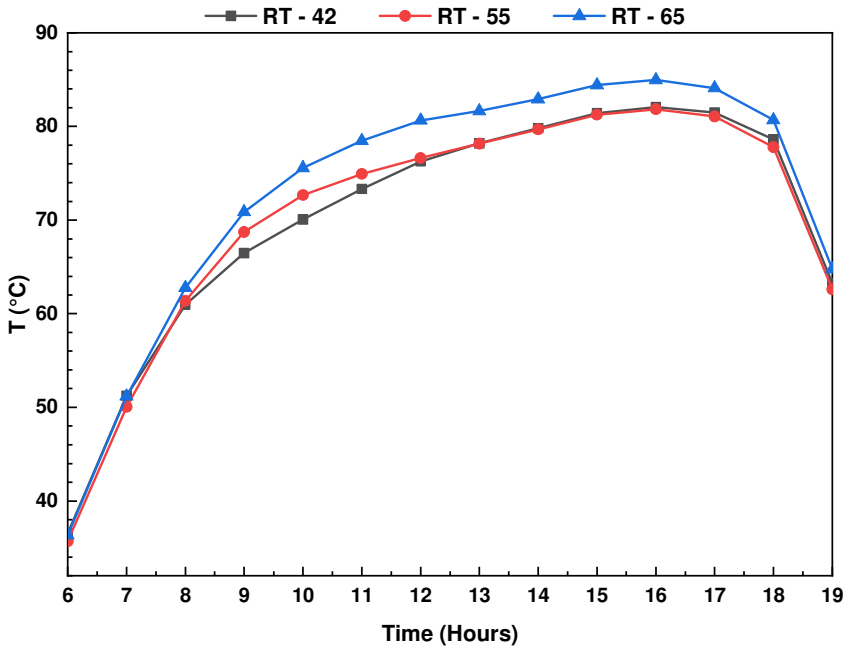

Fig.19 Time wise variation of water temperature during the charging process.

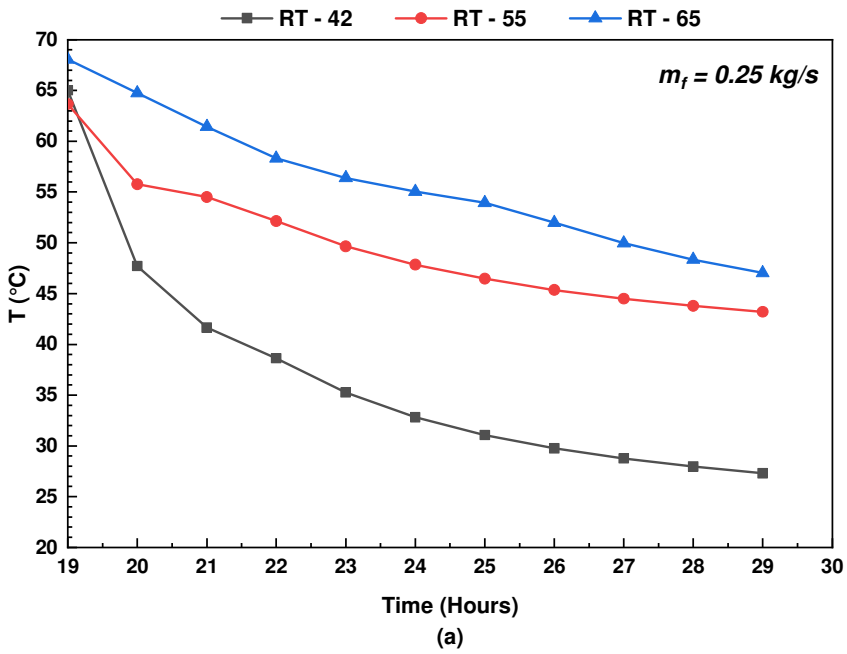
RT - 42
RT - 55
RT - 65
m_f = 0.25 kg/s
T (°C)
Time (Hours)

(a)

1

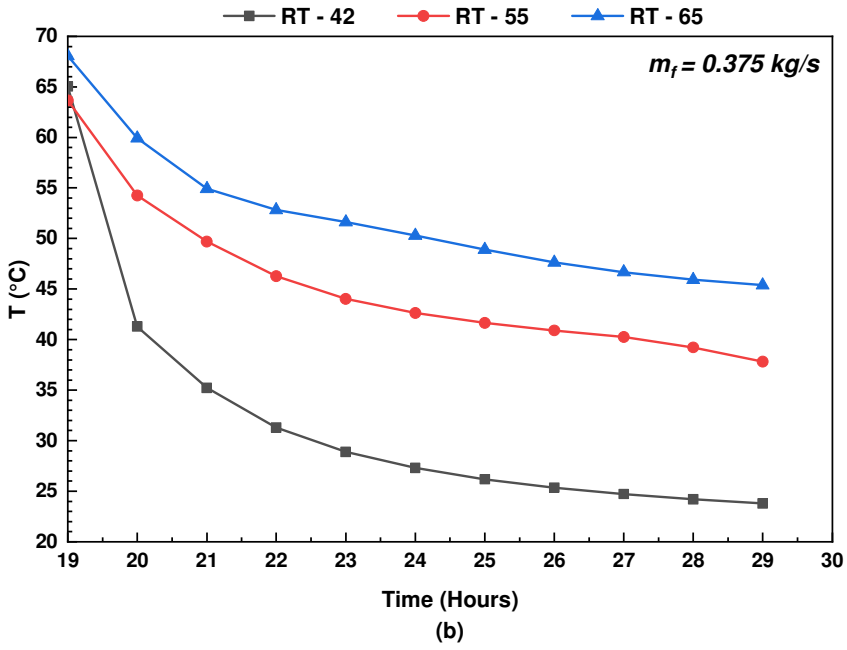
RT - 42
RT - 55
RT - 65
m_f = 0.375 kg/s
T (°C)
Time (Hours)

(b)

2

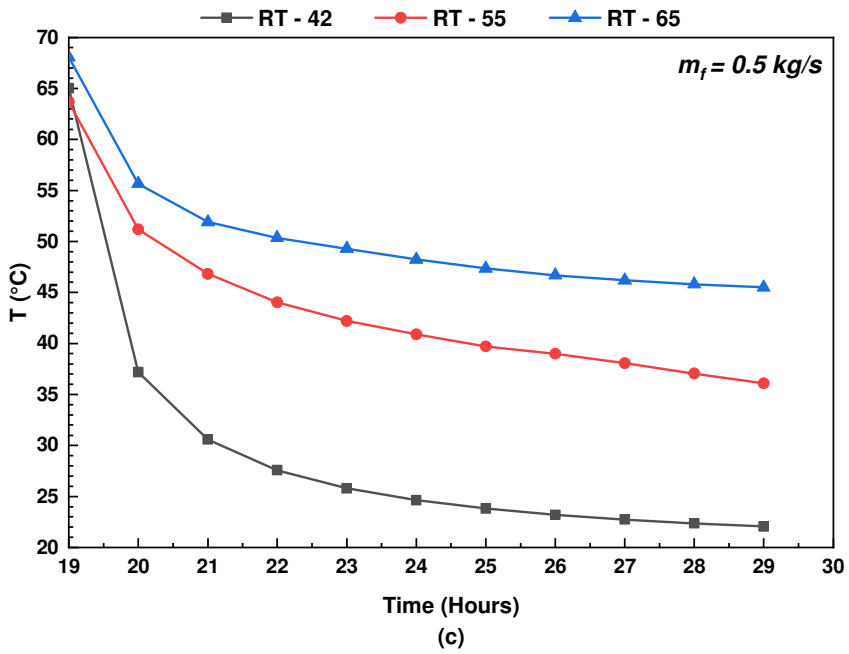

Fig.20 Time wise variation of water temperature during the discharging process for three different mass flow rates: 0.25 kg/s (a), 0.375 kg/s (b) and 0.5 kg/s (c).

Finally, it can be concluded that the proposed SPTC-LHTES is suitable for large buildings with high consumption rate of hot water (up to 1800 l/h) and it is able to produce hot water within the ranges of 85-36 °C and 63-38 °C, during daytime and nighttime operation, respectively. It is worth noting that in large buildings (hotels, hospitals, barracks, etc), the amount of SHWs is generally high which require a large space and the roofs of these buildings are not always enough to allocate these solar panels. To overcome this problem, it is recommended to use available unshaded ground space around these type of buildings and the proposed system can be successfully ground mounted.

6. Conclusion

In the present work, a novel solar water heater with heat storage in PCM is proposed for large buildings hot water production such as hotels, hospitals, barracks, etc. The studied system is composed mainly of a solar parabolic through collector (SPTC) coupled with a shell and tube latent heat thermal energy storage (LHTES) system and a circulation pump. A detailed thermal dynamic model is developed for investigating the performance of the coupled SPTC-LHTES under realistic weather conditions and it is validated with existent experimental and numerical results. The maximal discrepancy between numerical results and experimental data does not exceed 5 %. The optimal design of the LHTES is determined for a typical

summer day in Ajaccio city in the south of France. The effect of both water mass flow rate and the PCM type on the produced water temperature during the discharging process is presented and discussed. The main findings of the present work can be summarized as the following:

- Using the solar concentrator (SPTC) as solar water heater is able to produced hot water in the range of 85-36 °C and with a suitable mass flow rate for large building (up to 1800 l/h) during the sunshine hours.
- Maximal useful heat by water in the SPTC with an area of 100 m² during the daytime operation is about 72.6 kW and it is reached at noon.
- The proposed storage system in PCM is coupled with the SPTC and it is able to store thermal energy during the sunshine hours and to release it to the cold water during the off-sunshine hours;
- Maximal amount of stored latent heat in PCM at the end of the charging process is 2.24 times greater than that stored into sensible form.
- The mass flow rate of water and the PCM melting temperature have a significant effect on the water temperature during the nighttime system operation;
- Increasing the mass flow rate from 0.25 kg/s to 0.5 kg/s during nighttime operation of the system leads to decrease the average outlet water temperature by about 30 %.
- The amount of latent heat stored at the end of the charging process is 1860 MJ, 1592.68 MJ and 1134.45 MJ for RT-42, RT-55 and RT-65, respectively.
- For a high consumption rate of hot water (about 1800 l/h), using RT-55 as PCM in the studied SPTC-LHTES is suitable compared to RT-42 and RT-65.
- The proposed SPTC-LHTES is suitable for large buildings hot water production and it is able to produce hot water within the ranges of 85-36 °C and 63-38 °C, during daytime and nighttime operation, respectively.

As perspectives of the present study, the heat transfer enhancement techniques of the LHTES and economic and environment assessment of the proposed coupled SPTC-LHTES system will be investigated and presented in future research works .

Nomenclature

A	Area (m²)	**Subscript**	
a	Thermal diffusivity (m^2/s)	A	Absorber
C_p	Heat capacity (J/kg K)	ab	Absorbed
D	Diameter (m)	amb	Ambient
f	Liquid fraction (-)	c	Collector
$\bar{f}$	Liquid fraction at the end of the charging process (-)	cv	Convection
f_r	Friction factor (-)	ext	Exterior
h	Enthalpy (J/m^3) or heat transfer coefficient (W/m^2K)	f	Fluid
H	Length of the storage system (m)	i	Inner
I_d	Direct normal irradiance on the collector (W/m^2)	In	Inlet
k	Thermal conductivity (W/m K)	int	Interior
L	Length of the solar collector (m)	l	Liquid
L_s	Latent heat of fusion (J/kg)	m	Phase change material
M_{PCM}	Mass of phase change material (kg)	mel	Melting
$\dot{m}_f$	Mass flow rate of water (kg/s)	o	Outlet
N_p	Number of tubes in the storage system(-)	r	Radiation
P_r	Prandtl number (-)	s	Solid
Q	Heat rate (W)	st	Stored
$\dot{Q}$	Thermal energy (J)	u	Useful
r	Radial coordinate (m)	V	Glass cover
r_i	Inner radius (m)	sky	Sky
r_e	Outer radius (m)	**Abbreviations**	
R_e	Reynolds number (-)	DNI	Direct normal irradiance
T	Temperature (K or °C)	ETC	Evacuated tube collector
t	Time (s)	FPC	Flat plate collector
v	Velocity (m/s)	HTF	Heat transfer fluid
V_{PCM}	Volume of phase change material (m^3)	LHTES	Latent heat thermal energy storage
W	Width of the solar collector (m)	PCM	Phase change material
X	Axial coordinate (m)	SPTC	Solar parabolic through collector
Greek symbols		SWH	Solar water heater
α	Absorptance coefficient (-)		
τ	Transmittance coefficient (-)		
γ	Intercept factor (-)		
ε	Emittance (-)		
ρ	Density (kg/m^3)		
ρ_m	Reflectivity of surface (-)		
μ	Dynamic viscosity [Pa.s]		
σ	Stefan–Boltzmann constant (W/m^2K^4)		
η	Efficiency (-)		
Δr	Radial space step (m)		
Δx	Axial space step (m)		

Appendix

The heat transfer coefficients used the SPTC numerical model are taken from [33] and [49] and are given as the following:

- Convective heat transfer coefficient between the heat transfer fluid and the absorber tube:

$$h_{cv,f} = \begin{cases} \dfrac{k_f}{D_i} 4.36 & R_e \leq 2300 \\ \dfrac{k_f}{D_i}\left(\dfrac{\left(\frac{f_r}{8}\right)(R_e - 1000)P_r}{1 + 12.7\left(\frac{f_r}{8}\right)^{0.5}\left((P_r)^{\frac{2}{3}} - 1\right)}\right) & R_e > 2300 \end{cases} \quad \text{(A1)}$$

Where R_e and P_r are the Reynolds and the Prandtl numbers. $f_r$is the friction factor expressed as :

$$f_r = (1.82 log_{10}(R_e) - 1.64)^{-2} \quad \text{(A2)}$$

- Convective heat transfer coefficient between the ambient air and the external surface of the glass cover:

$$h_{cv,ext} = 4\, v_{ext}^{0.58} D_{V,ext}^{-0.42} \quad \text{(A3)}$$

Where v_{ext} and D_e are the wind speed and the external diameter of the receiver glass cover, respectively.

- Radiation heat transfer coefficient between the absorber and glass cover:

$$h_{r,int} = \frac{\sigma((T_A)^2 + (T_V)^2)(T_A + T_V)}{\frac{1}{\varepsilon_A} + \frac{1 - \varepsilon_V}{\varepsilon_V}\left(\frac{D_A}{D_{V,int}}\right)} \quad \text{(A4)}$$

Where ε and σ are the emittance the Stefan–Boltzmann constant, respectively.

- Radiation heat transfer coefficient between the glass cover and the sky:

$$h_{r,ext} = \sigma\varepsilon_v\left((T_V)^2 + \left(T_{Sky}\right)^2\right)\left(T_{Sky} + T_V\right) \quad \text{(A5)}$$

References

[1] IEA – International Energy Agency 2020. https://www.iea.org/topics/buildings.

[2] Pomianowski MZ, Johra H, Zhang C. Sustainable and energy-efficient domestic hot water systems : A review. Renew Sustain Energy Rev 2020;128:109900. doi:10.1016/j.rser.2020.109900.

[3] Jamar A, Majid ZAA, Azmi WH, Norhafana M, Razak AA. A review of water heating system for solar energy applications. Int Commun Heat Mass Transf 2016;76:178–87. doi:10.1016/j.icheatmasstransfer.2016.05.028.

[4] Evangelisti L, De Lieto Vollaro R, Asdrubali F. Latest advances on solar thermal collectors: A comprehensive review. Renew Sustain Energy Rev 2019;114:109318. doi:10.1016/j.rser.2019.109318.

[5] Gautam A, Chamoli S, Kumar A, Singh S. A review on technical improvements, economic feasibility and world scenario of solar water heating system. Renew Sustain Energy Rev 2017;68:541–62. doi:10.1016/j.rser.2016.09.104.

[6] Yılmaz İH. Residential use of solar water heating in Turkey: A novel thermo-economic optimization for energy savings, cost benefit and ecology. J Clean Prod 2018;204:511–24. doi:10.1016/j.jclepro.2018.09.060.

[7] Allouhi A, Jamil A, Kousksou T, El Rhafiki T, Mourad Y, Zeraouli Y. Solar domestic heating water systems in Morocco: An energy analysis. Energy Convers Manag 2015;92:105–13. doi:10.1016/j.enconman.2014.12.055.

[8] Rankin R, Rousseau PG. Sanitary hot water consumption patterns in commercial and industrial sectors in South Africa: Impact on heating system design. Energy Convers Manag 2006;47:687–701. doi:10.1016/j.enconman.2005.06.002.

[9] Kitzberger T, Kilian D, Kotik J, Pröll T. Comprehensive analysis of the performance and intrinsic energy losses of centralized Domestic Hot Water (DHW)systems in commercial (educational)buildings. Energy Build 2019;195:126–38. doi:10.1016/j.enbuild.2019.05.016.

[10] Bujak J. Heat consumption for preparing domestic hot water in hospitals. Energy Build 2010;42:1047–55. doi:10.1016/j.enbuild.2010.01.017.

[11] Fuentes E, Arce L, Salom J. A review of domestic hot water consumption profiles for

application in systems and buildings energy performance analysis. Renew Sustain Energy Rev 2018;81:1530–47. doi:10.1016/j.rser.2017.05.229.

[12] Pedersen P. Experience with a large solar DHW system in denmark--The nordic solar heating demonstration project 1993;50:259–66.

[13] Pedersen P V. System design optimization for large building integrated solar heating systems for domestic hot water. Sol Energy 1993;50:267–73. doi:10.1016/0038-092X(93)90020-O.

[14] Ndoye B, Sarr M. Analysis of domestic hot water energy consumption in large buildings under standard conditions in Senegal. Build Environ 2008;43:1216–24. doi:10.1016/j.buildenv.2007.02.012.

[15] Colmenar-Santos A, Vale-Vale J, Borge-Diez D, Requena-Pérez R. Solar thermal systems for high rise buildings with high consumption demand: Case study for a 5 star hotel in Sao Paulo, Brazil. Energy Build 2014;69:481–9. doi:10.1016/j.enbuild.2013.11.036.

[16] Fertahi S ed D, Jamil A, Kousksou T, Benbassou A. Energy performance enhancement of a collective hot water production process equipped with a centralized storage tank. J Energy Storage 2019;25:100849. doi:10.1016/j.est.2019.100849.

[17] Kalogirou SA, Lloyd S. Use of solar Parabolic Trough Collectors for hot water production in Cyprus. A feasibility study. Renew Energy 1992;2:117–24. doi:10.1016/0960-1481(92)90097-M.

[18] Steven A. Parker. Parabolic-Trough Solar Water Heating. Washington: 2000. doi:DOE/GO-102000-0973.

[19] Fernández-García A, Zarza E, Valenzuela L, Pérez M. Parabolic-trough solar collectors and their applications. Renew Sustain Energy Rev 2010;14:1695–721.

[20] Zou B, Dong J, Yao Y, Jiang Y. An experimental investigation on a small-sized parabolic trough solar collector for water heating in cold areas. Appl Energy 2016;163:396–407. doi:10.1016/j.apenergy.2015.10.186.

[21] Allouhi A, Benzakour Amine M, Kousksou T, Jamil A, Lahrech K. Yearly performance of low-enthalpy parabolic trough collectors in MENA region according to different sun-tracking strategies. Appl Therm Eng 2018;128:1404–19. doi:10.1016/j.applthermaleng.2017.09.099.

[22] Soudani ME, Aiadi KE, Bechki D. Water heating by Parabolic Trough Collector with storage in the Ouargla region of Algerian Sahara. Mater Today Proc 2019:10–2. doi:10.1016/j.matpr.2019.07.707.

[23] Kumar D, Kumar S. Year-round performance assessment of a solar parabolic trough collector under climatic condition of Bhiwani, India: A case study. Energy Convers Manag 2015;106:224–34. doi:10.1016/j.enconman.2015.09.044.
[24] Kalogirou SA. Parabolic trough collectors for industrial process heat in Cyprus. Energy 2002;27:813–30. doi:10.1016/S0360-5442(02)00018-X.
[25] Jaramillo OA, Borunda M, Velazquez-Lucho KM, Robles M. Parabolic trough solar collector for low enthalpy processes: An analysis of the efficiency enhancement by using twisted tape inserts. Renew Energy 2016;93:125–41. doi:10.1016/j.renene.2016.02.046.
[26] Seddegh S, Wang X, Henderson AD, Xing Z. Solar domestic hot water systems using latent heat energy storage medium: A review. Renew Sustain Energy Rev 2015;49:517–33. doi:10.1016/j.rser.2015.04.147.
[27] Zayed ME, Zhao J, Elsheikh AH, Hammad FA, Ma L, Du Y, et al. Applications of cascaded phase change materials in solar water collector storage tanks: A review. Sol Energy Mater Sol Cells 2019;199:24–49. doi:10.1016/j.solmat.2019.04.018.
[28] Elbahjaoui R, El Qarnia H. Thermal performance of a solar latent heat storage unit using rectangular slabs of phase change material for domestic water heating purposes. Energy Build 2019;182:111–30. doi:10.1016/j.enbuild.2018.10.010.
[29] Teamah HM, Lightstone MF, Cotton JS. Potential of cascaded phase change materials in enhancing the performance of solar domestic hot water systems. Sol Energy 2018;159:519–30. doi:10.1016/j.solener.2017.11.034.
[30] Haillot D, Franquet E, Gibout S, Bédécarrats JP. Optimization of solar DHW system including PCM media. Appl Energy 2013;109:470–5. doi:10.1016/j.apenergy.2012.09.062.
[31] Luu MT, Milani D, Nomvar M, Abbas A. Dynamic modelling and analysis of a novel latent heat battery in tankless domestic solar water heating. Energy Build 2017;152:227–42. doi:10.1016/j.enbuild.2017.07.020.
[32] Abdelsalam MY, Teamah HM, Lightstone MF, Cotton JS. Hybrid thermal energy storage with phase change materials for solar domestic hot water applications: Direct versus indirect heat exchange systems. Renew Energy 2020;147:77–88. doi:10.1016/j.renene.2019.08.121.
[33] Lamrani B, Khouya A, Zeghmati B, Draoui A. Mathematical modeling and numerical simulation of a parabolic trough collector: A case study in thermal engineering. Therm Sci Eng Prog 2018;8:47–54. doi:10.1016/j.tsep.2018.07.015.

[34] Bellos E, Tzivanidis C. Alternative designs of parabolic trough solar collectors. Prog Energy Combust Sci 2019;71:81–117. doi:10.1016/j.pecs.2018.11.001.
[35] Lamrani B, Khouya A, Draoui A. Energy and environmental analysis of an indirect hybrid solar dryer of wood using TRNSYS software. Sol Energy 2019;183:132–45. doi:10.1016/j.solener.2019.03.014.
[36] Kalogirou SA. Solar thermal collectors and applications. Prog Energy Combust Sci 2004;30:231–95.
[37] Lamrani B, Draoui A. Modelling and simulation of a hybrid solar-electrical dryer of wood integrated with latent heat thermal energy storage system. Therm Sci Eng Prog 2020;18:100545. doi:10.1016/j.tsep.2020.100545.
[38] Kuznik F, Johannes K, Franquet E, Zalewski L, Gibout S, Tittelein P, et al. Impact of the enthalpy function on the simulation of a building with phase change material wall. Energy Build 2016;126:220–9. doi:10.1016/j.enbuild.2016.05.046.
[39] Lacroix M. Study of the heat transfer behavior of a latent heat thermal energy storage unit with a finned tube. Int J Heat Mass Transf 1993;36:2083–92. doi:10.1016/S0017-9310(05)80139-5.
[40] Adine HA, El Qarnia H. Numerical analysis of the thermal behaviour of a shell-and-tube heat storage unit using phase change materials. Appl Math Model 2009;33:2132–44. doi:10.1016/j.apm.2008.05.016.
[41] Elbahjaoui R, Qarnia H El, Naimi A. Energy & Buildings Thermal performance analysis of combined solar collector with triple concentric-tube latent heat storage systems. Energy Build 2018;168:438–56. doi:10.1016/j.enbuild.2018.02.055.
[42] Trp A. An experimental and numerical investigation of heat transfer during technical grade paraffin melting and solidification in a shell-and-tube latent thermal energy storage unit. Sol Energy 2005;79:648–60. doi:10.1016/j.solener.2005.03.006.
[43] Mostafavi SS, Taylor RA, Saberi P, Diarce G. Design and feasibility of high temperature shell and tube latent heat thermal energy storage system for solar thermal power plants. Renew Energy 2016;96:120–36. doi:10.1016/j.renene.2016.04.036.
[44] Ding C, Niu Z, Li B, Hong D, Zhang Z, Yu M. Analytical modeling and thermal performance analysis of a flat plate latent heat storage unit. Appl Therm Eng 2020;179:115722. doi:10.1016/j.applthermaleng.2020.115722.
[45] Gnielinski V. On heat transfer in tubes. Int J Heat Mass Transf 2013;63:134–40.
[46] Voller VR. Fast implicit finite-difference method for the analysis of phase change problems. Numer Heat Transf 1990;17:155–69.

[47] Dudley V, Kolb G, Mahoney A, Mancini T, Mattews C, Sloan M. Test results: SEGS LS-2 solar collector. Report of Sandia National Laboratories (SAND94-1884). 1994.
[48] Peter K. A guide to the standard EN 12975. 2012.
[49] Naeeni N, Yaghoubi M. Analysis of wind flow around a parabolic collector (2) heat transfer from receiver tube. Renew Energy 2007;32:1259–72. doi:10.1016/j.renene.2006.06.005.